NACA RM A54L27

NACA

RESEARCH MEMORANDUM

A FLIGHT INVESTIGATION AT TRANSONIC SPEEDS OF A MODEL HAVING A TRIANGULAR WING OF ASPECT RATIO 4

By Loren G. Bright

Ames Aeronautical Laboratory
Moffett Field, Calif.

NATIONAL ADVISORY COMMITTEE
FOR AERONAUTICS

WASHINGTON

March 24, 1955
Declassified January 20, 1958

NATIONAL ADVISORY COMMITTEE FOR AERONAUTICS

RESEARCH MEMORANDUM

A FLIGHT INVESTIGATION AT TRANSONIC SPEEDS OF A MODEL HAVING A TRIANGULAR WING OF ASPECT RATIO 4

By Loren G. Bright

SUMMARY

Free-falling recoverable-model tests have been conducted at transonic speeds on a model having an aspect-ratio-4 triangular wing and a 45° sweptback tail located in the extended wing-chord plane. Static- and dynamic-stability and load-distribution data were obtained at maximum angles of attack of about 8° to 21°, depending on the Mach number. As angle of attack was varied, at subsonic values of Mach number, the aerodynamic center of the complete model moved one-half the mean aerodynamic chord as a result of the reduced stability contributions of both wing and tail at low angles of attack. Lowered values of horizontal-tail effectiveness for values of Mach number above 0.99 are believed to result from losses of dynamic pressure in the wing wake. Large losses of damping in pitch at high angles of attack, noted at Mach numbers less than 0.92, were probably due to nonlinear variations with angle of attack of the downwash angle at the tail.

INTRODUCTION

A series of tests of freely falling models has provided data on models at transonic speeds and at Reynolds numbers approximating those of full-scale airplanes. In these tests a model having an aspect-ratio-4 triangular wing has been investigated. In references 1, 2, and 3, similar wings have been tested at Mach numbers from 0.30 to 0.96 and from 1.2 to 1.7, and at Reynolds numbers up to 4 million. The results of this report differ from the wind-tunnel tests in these respects:

1. Transonic Mach numbers were covered. The Mach number ranged from 0.88 to 1.14.

2. The tests were made at higher Reynolds numbers. Reynolds numbers ranged from 8.3 million to 16.2 million.

3. Load distribution over the model was measured.

4. Dynamic stability characteristics of the model were obtained.

The tests were made by Ames Aeronautical Laboratory using the recoverable free-fall model technique in an area provided by the Air Force at Edwards Air Force Base, Edwards, California.

SYMBOLS

b	wing span, ft
c	local wing chord, ft
$\bar{c}$	mean aerodynamic chord of the wing, $\frac{2}{S}\int_0^{b/2} c^2 dy$, ft
I_y	moment of inertia of the model about the Y axis, slug-ft^2
M	Mach number
m	twisting couple applied at wing tip, ft-lb
p	static pressure at a fuselage orifice, lb/sq ft
q	rate of pitch, radians/sec
q_o	dynamic pressure, lb/sq ft
q_t	dynamic pressure at horizontal tail, lb/sq ft
$\dot{q}$	angular acceleration in pitch, radians/sec^2
r	radius of fuselage at longitudinal station x, in.
S	wing area, including portion of wing covered by fuselage, sq ft
x	longitudinal distance from fuselage station 0, in.
y	spanwise distance from model center line, ft
V	speed, ft/sec
C_D	drag coefficient, based on wing area
C_L	lift coefficient, based on wing area

C_m pitching-moment coefficient, based on wing area and mean aerodynamic chord

C_{m_t} pitching-moment coefficient due to tail

α angle of attack, deg

$\dot{\alpha}$ rate of change of angle of attack, radians/sec

β angle of sideslip, deg

δ deflection of horizontal tail, deg

ϵ downwash angle, deg

θ angle of twist, deg

Subscripts

e exposed wing panels

l lower

q rate of pitch, $\frac{q\bar{c}}{2V}$

T complete model

u upper

w total wing

max maximum

min minimum

$\dot{\alpha}$ rate of change of angle of attack, $\frac{\dot{\alpha}\bar{c}}{2V}$

α,β,δ derivative of the factor with respect to the subscript, as

$$C_{L_\alpha} = \frac{\partial C_L}{\partial \alpha}, \text{ etc.}$$

MODEL

A dimensional sketch of the complete model is shown in figure 1 and additional pertinent dimensions are listed in table I. A photograph of the model with booster attached, taken immediately after release from

the drop airplane, is shown in figure 2. The rocket booster was used in some of the tests to obtain higher Mach numbers.

The wing of the model was of the same plan form (aspect-ratio-4 triangular) as that of the wings of references 1, 2, and 3. The airfoil section was NACA 0005 parallel to free stream (table II). The wing panels were constructed of a composite steel core with a built-up wood surface. Mounting the wing panels in a strain-gage balance to measure exposed wing loads necessitated a gap at the wing-root-fuselage juncture, which was sealed by a flexible rubber seal to prevent air flow into and out of the fuselage and from lower to upper wing surface.

Remaining model components were as described in references 4 and 5.

INSTRUMENTATION

The following information was continuously recorded by two oscillographs:

Quantity	Transducer
Angles of attack and sideslip	Selsyns geared to vanes mounted on boom ahead of model (fig. 1)
Vertical and longitudinal acceleration	Statham linear accelerometers
Angular acceleration in pitch	Statham angular accelerometer
Wing balance loads	Strain gages (see ref. 4 for details)

The following information was recorded continuously by NACA standard flight instruments:

Quantity	Recorder
Pitching and rolling velocity	NACA two-component turnmeter
Angular position of horizontal- and vertical-tail surfaces	NACA two-component control position recorder
Mach number and dynamic pressure	NACA six-cell manometer
Differential pressure between orifices on upper and lower surfaces of fuselage	NACA six-cell manometers
Deflection of wing-tip	16-mm GSAP movie camera mounted in fuselage and sighting along wing span

All the flight records were synchronized by a chronometric timer. The airspeed system was calibrated in flight at different angles of attack using the SCR 584 tracking radar installation of the NACA High-Speed Flight Station at Edwards Air Force Base.

TESTS

The test procedure used was the same as that described in references 4 and 5, that is, after attaining the test Mach number, the horizontal control was intermittently pulsed according to a preset schedule, and data were recorded during the concomitant oscillations. In addition, for some drops, rocket assist was employed in order to increase the attainable Mach number. The booster rocket (fig. 2) was jettisoned at the conclusion of the boost phase and prior to the actual test period.

The results presented herein were obtained in seven drops and cover a Mach number range from 0.88 to 1.14, and a Reynolds number range from 8.3 million to 16.2 million (fig. 3). The angle-of-attack range of these tests was from -1° to 21° for Mach numbers less than 1.02, and angles of attack from 0° to about 10° for Mach numbers greater than 1.02.

Supplementary ground tests were also made (Appendix) to determine the deflection characteristics of the wing. The elastic-axis location and the torsional stiffness of the wing were determined by applying a twisting couple near the wing tip. Influence coefficients were determined by applying concentrated loads and measuring wing deflections at various points on the wing (table III).

Precision of Measurement

The instruments used in the present investigation were of the same accuracy as those used in the tests of reference 4. The error of any single value of the angle of attack or Mach number was equal to the values given in reference 4, and the error of any single value of an aerodynamic coefficient is altered by the ratio of appropriate wing dimensions. Application of these factors yields the following values:

Item	Estimated maximum errors	
	M = 0.85	M = 1.05
C_{L_T}	±0.01	±0.005
C_{L_e}	±.01	±.004
C_{D_T}	±.0006	±.0003
C_{D_e} and C_{D_w}	±.002	±.001
C_{m_T}	±.001	±.001
$C_{m_{(\bar{c}/4)e}}$ and $C_{m_{(\bar{c}/4)w}}$	±.001	±.001
Mach number	±.01	±.01
Angle of attack	±1/4°	±1/4°

RESULTS

In general, the flight data were evaluated by the methods described in references 4 and 5. The results are identified as applying to the following:

1. The exposed wing panels.

2. The total wing, obtained by adding to the data for the exposed wing panels, the data obtained by integrating the pressure differences over the fuselage between stations 51 and 135. An additional total wing drag increment was obtained by applying a skin-friction coefficient of 0.0028 to the entire fuselage surface area between stations 51 and 135.

3. The total model.

Lift

In figure 4 curves are presented of lift coefficient as a function of angle of attack for the test range of Mach numbers. In figure 5, the lift-curve slopes for the various model components are plotted as a function of Mach number. The lift-curve slopes for the complete model were determined at the smallest value of horizontal-tail setting, δ, for which data were available ($|\delta| \leq 4^\circ$ in all cases).

DRAG

Variation of C_D with C_L is presented in figure 6 for various Mach numbers. The drag curves were obtained in two tests, one of which yielded the variation of C_D with C_L but was in error by an increment resulting from one of the model hangars not being completely retracted. A second test at zero angle of attack provided minimum drag data with which the first test was corrected. In figure 7 are plotted, as a function of Mach number, the values of the drag-rise factor $\partial C_D/\partial C_L^2$ (at zero lift) for the total wing and total model, and the values of $C_{D_{min}}$ for the total model.

Static Longitudinal Stability

Curves showing the variation of the trim angle of attack with Mach number for several horizontal-tail settings are presented in figure 8.

The variation of complete model pitching-moment coefficient, C_{m_T}, with α has been computed for several values of Mach number at $\delta = 0^\circ$, and is presented in figure 9. The data have been corrected for center-of-gravity location and horizontal-tail setting, assuming that tail stability contribution is independent of tail load and that there are no discontinuities in the C_{m_T} curves.

Values of C_{m_T} were determined from the expression

$$C_{m_T} = \frac{I_y \dot{q}}{q_o S \bar{c}} - C_{m_q} \frac{q\bar{c}}{2V} - C_{m_{\dot{\alpha}}} \frac{\dot{\alpha}\bar{c}}{2V}$$

assuming the contribution of the damping terms to be negligibly small, that is, $C_{m_T} = I_y \dot{q}/q_o S \bar{c}$. (In these tests the error in making this assumption was found to be less than 0.5 percent.) Included in this figure are curves of total-wing pitching-moment coefficient, C_{m_w}, for the same center-of-gravity location.

Shown, in addition, in figure 9 are curves of C_{m_t} - determined by subtracting from the complete-model data the data for the total wing. It should be noted that this method of evaluating C_{m_t} includes the contribution to C_{m_T} of that portion of the fuselage not included in the region where pressures were measured. The magnitude of this contribution in relation to that of the tail is considered negligible.

Cross plots of wing pitching moment about the quarter-chord point of the wing mean aerodynamic chord are shown in figure 10 for the exposed wing panels, C_{m_e} vs. C_{L_e}, and the total wing, C_{m_w} vs. C_{L_w}, for several

values of Mach number. Included for comparison are similar results from references 2 and 3.

The variations of aerodynamic-center location with Mach number for various model components are shown in figure 11(a). Marked differences in longitudinal stability between "low" and "high" angle-of-attack ranges were noted in the data. The values of C_L at which these changes occurred are presented as a function of Mach number in figure 11(b).

Dynamic Longitudinal Stability

Values of the damping-in-pitch parameter, $C_{m_q} + C_{m_{\dot{\alpha}}}$, are shown in figure 12 as a function of Mach number. The data were obtained by deducting the contribution of the lift-curve slope from the total damping factor obtained by analysis of the control-fixed oscillations of the model.

Horizontal-Tail Effectiveness

In figure 13 is shown the variation with Mach number of the horizontal-tail-effectiveness parameter, C_{m_δ}. Two methods were used to evaluate this parameter. One method was to obtain the slope of a plot of C_{m_T} against δ during a control pulse choosing data for these periods during which α remained fairly constant. The second method was to plot as a function of $\Delta\delta_{trim}$ the change in C_{m_T} required to aline the curves of C_{m_T} vs. α for $\delta \neq 0^\circ$ with those for $\delta = 0^\circ$.

Loading Distribution Over Fuselage

In figure 14 are presented distributions of fuselage loading along the lines of intersection of the fuselage surface with the plane of symmetry and with a plane rotated 45° from the plane of symmetry about the fuselage center line. The locations of the orifices from which the data were obtained are shown in figure 15. The data represent the differences in pressure coefficient between corresponding orifices on the upper and lower surfaces of the fuselage.

Buffet Boundary

All flight records were examined for indications of buffeting, and the lift coefficient for the complete model at which buffeting initially occurred is plotted as a function of Mach number in figure 16. This

buffet boundary is herein defined as that point at which the character of the normal accelerometer record changes from its steady lift appearance to one of aperiodic, unsteady fluctuations. Since the instrumentation used in this investigation was primarily selected to obtain information other than buffeting, further quantitative analysis of the data was not considered justified.

DISCUSSION

Lift

The lift curves of figure 4 show some nonlinearities and failure to pass through zero at $\alpha = 0^{\circ}$ in the range of Mach numbers from 0.98 to 1.02. These nonlinearities should be further investigated since few data are presently available in this Mach number range.

The lift-curve slopes for the wing of the present tests have been compared with the results of references 1, 2, and 3 in figure 17. As shown, the present values are somewhat lower than those obtained in other tests at lower values of Reynolds number (1.5×10^{6} to 4.0×10^{6}), although the variations with Mach number are similar. This difference in lift-curve slope, as obtained from flight measurements and references 1 and 2, has been apparent in previous tests, reported in reference 6. The effect of aeroelastic deflection on wing lift was considered as a possible explanation of this difference, but ground tests of the wing deflection and twist, described in the Appendix, indicated that this effect was insignificant. The cause of the difference is unresolved at this time.

Drag

In figures 7(a) and 7(b), the experimental drag rise with lift, in terms of the factor $\partial C_D/\partial C_L{}^2$, is compared with values computed assuming (1) full leading-edge suction and (2) the resultant force vector perpendicular to the wing chord $1/57.3C_{L_\alpha}$. The results indicate that the wing realizes from 10- to 20-percent leading-edge suction throughout the range of these tests. Values of the factor $\partial C_D/\partial C_L{}^2$ were somewhat smaller for the complete model than for the wing. Since the main difference between the two configurations is the horizontal tail, this comparison indicates that the tail develops lift with a smaller drag penalty than does the wing.

The curves of figure 7(c) present a comparison of the flight variation of minimum drag coefficient with Mach number to that computed theoretically by adding to the subsonic drag value the incremental drag rise

determined by the method of reference 7. Good agreement between experimental results and theory is to be noted.

Static Longitudinal Stability

Throughout the test range of Mach numbers, the data of figure 11(a) for the complete model indicate the aerodynamic center to be farther aft at high lift coefficients than at low lift coefficients. This shift in aerodynamic-center location is shown to be greatest, about $0.52\bar{c}$, at Mach numbers less than 0.94, while at Mach numbers greater than 1.00 the shift is reduced to about $0.05\bar{c}$. The angle of attack at which these shifts in aerodynamic-center location occur is rather sharply defined (fig. 9) and decreases progressively with increasing Mach number from 15° at $M = 0.92$ to about 3° at $M = 1.07$. The values of lift coefficient at which the change in stability occurs is shown as a function of Mach number in figure 11(b).

The stability variations with angle of attack for the complete model are believed due to changes in the stability contributions of both the wing-fuselage combination and the tail for values of Mach number up to 1.08 (fig.9). The tail stability contribution, for instance, increases from nearly zero at low angles of attack to substantial values at higher angles of attack for the Mach number range considered. (It is of interest, also, to note the very small change in aerodynamic-center location from wing to total model at small angles of attack and the relatively large change in aerodynamic-center location at high angles of attack in fig. 11(a).) The horizontal-tail-effectiveness data of figure 13 do not indicate sufficient influence of angle of attack to account for the observed change in tail contribution to stability; hence, the product $C_{L_{\alpha_t}}(q_t/q_o)$ cannot be charged with the change. The downwash studies of references 8 and 9 indicate large values of $\partial\epsilon/\partial\alpha$ at high subsonic speeds for angles of attack up to about 10° ($C_L = 0.8$). At higher values of α the downwash angle slope, $\partial\epsilon/\partial\alpha$, drops rapidly to a low value. This would account for the marked changes in tail contribution to total model stability shown in figure 9. The tail-location studies of reference 10 indicate that a slightly higher tail location could defer the increase in tail contribution to model stability to a higher angle of attack by placing the tail in a more favorable downwash field. This is seen as a possible means of reducing the very large aerodynamic-center travel.

The stability contribution of the total wing decreases at moderate angles of attack, compensating for increases in tail contribution. At Mach numbers less than 0.95, another break occurs in the total-wing stability curves at high angles of attack - this time, stabilizing. This final slope, augmenting the increased contribution of the tail, produces the large aerodynamic-center shift noted at the lower Mach numbers in figure 11(a).

The variation with Mach number of the wing aerodynamic-center location at low lift coefficients is compared in figure 18 with those of models having similar wings reported in references 1, 2, and 3. The flight results are seen to be in good agreement with the results of other test facilities.

Dynamic Longitudinal Stability

The longitudinal damping characteristics of the flight model are indicated by the $C_{m_q} + C_{m_{\dot{\alpha}}}$ data of figure 12. The model damping, which results principally from the tail, shows little variation with Mach number at low angles of attack. The general level of this curve is in good agreement with a computed curve based on the results of reference 11 plus the tail contribution as calculated by the method outlined in reference 5. Approximately 70 percent of the estimated model damping in pitch results from the tail contribution at values of Mach number below 0.92. At higher speeds the magnitude of the wing contribution is not known.

At Mach numbers greater than 0.96 there was little change in the damping with angle of attack. At subsonic Mach numbers and values of angle of attack greater than about 10°, however, the damping was reduced to a very low value. This probably results as the tail emerges from the wing wake at high angles of attack, causing a decrease in the damping due to rate of change of angle of attack, $C_{m_{\dot{\alpha}}}$. Analyses of airplane motions have shown that the lag in downwash angle at the tail is such as to make this portion of the complete damping coefficient, $C_{m_q} + C_{m_{\dot{\alpha}}}$, proportional to $1 + \partial\epsilon/\partial\alpha$. The effect of this emergence was also noted as a marked increase in tail contribution to model stability at high angles of attack in the foregoing discussion of static longitudinal stability.

Horizontal-Tail Effectiveness

Horizontal-tail-effectiveness data from these tests (fig. 13) agree reasonably well with results of references 5 and 6 (appropriately corrected for wing dimensions) which covered tests of the same tail located similarly but behind wings of different plan form. At Mach numbers greater than 0.97 the data show slightly lower values of C_{m_δ} than the results of reference 6. It will be noted that all data points in this range of Mach numbers were obtained at low angles of attack where the tail was presumably immersed in the wing wake. The reduced effectiveness is probably chargeable to a greater loss in dynamic pressure in the wing wake rather than to a reduction in lift-curve slope of the tail. The

higher values of C_{m_δ} shown for the tests of reference 5 were obtained at higher angles of attack where the tail would have emerged from the wing wake.

The curve through the present data has been omitted in the Mach number range from 0.93 to 0.97 since no data points are available in this region and previous similar tests (ref. 6) have shown erratic variations in horizontal-tail effectiveness at these speeds. An attempt was made to decrease the scatter of the horizontal-tail-effectiveness data determined from tail-pulse data reduction by applying corrections for rolling and yawing velocities, but the corrections were found to be of negligible magnitude.

Buffet Boundary

Some tendencies to buffet were noted in the flight records. The buffet boundary (fig. 16) is seen to increase steadily from a lift coefficient of 0.4 at Mach number of 0.86 to 0.6 at Mach number of 0.98 where it breaks sharply upward to a fairly constant value of about 0.95 for Mach numbers greater than 1.00.

In reference 12 studies of available data on low lift buffeting indicate that this phenomenon may be due to shock-induced separation of the wing flow. Over the range of the present tests, references 12 and 13 indicate similar trends toward an increase in the lift coefficient at which buffeting is initiated as Mach number is increased. This trend may occur as the wing normal shock wave becomes more stably located.

SUMMARY OF RESULTS

Flight tests conducted at transonic speeds with a free-falling model incorporating a triangular wing of aspect ratio 4 and a 45° sweptback horizontal tail located in the extended wing-chord plane showed the following results:

1. The lift-curve slopes for the total wing were less than corresponding values obtained on similar wings in combination with fuselages in other facilities, but the variations with Mach number were generally similar.

2. At subsonic speeds (Mach number less than about 0.98), the total model experienced a large shift in aerodynamic-center position as angle of attack was increased, amounting to approximately one half of the mean aerodynamic chord. At Mach numbers less than 0.95, the stability contributions of both the wing and the tail at low angles of attack were less

than at high angles of attack. This fact was at least partially responsible for the large aerodynamic-center shift. As the Mach number was increased above 0.94 the low and high angle-of-attack aerodynamic-center positions for the complete model converged rapidly, with the result that aerodynamic-center position was virtually unaffected by angle of attack at Mach numbers greater than 0.98.

3. The variation of the drag coefficient with lift at low lift was such as to indicate that the wing realizes from 10- to 20-percent leading-edge suction throughout the range of these tests.

4. Within the Mach number limits of the tests the buffet boundary was noted to rise gradually from a lift coefficient of 0.4 to 0.6 in the high subsonic speed range and then increase sharply to a fairly constant value of about 0.95 for Mach numbers greater than 1.00.

5. Changes in Mach number had little effect on the damping-in-pitch parameter, $C_{m_q} + C_{m_{\dot{\alpha}}}$, at low angles of attack and the level was generally consistent with predicted values. Very low damping in pitch was indicated for high angles of attack at Mach numbers less than about 0.92. Considerable variations in damping, noted in this speed range, are believed to result from the effect on tail damping of nonlinear variations of downwash angle with angle of attack.

6. The horizontal-tail-effectiveness characteristics at low angles of attack, and Mach numbers above 0.99, indicate values somewhat lower than those from previous tests of the same tail with three other wings. This is probably the result of an increased loss of dynamic pressure in the wing wake.

Ames Aeronautical Laboratory
National Advisory Committee for Aeronautics
Moffett Field, Calif., Dec. 27, 1954

APPENDIX

Ground tests were conducted on one of the test wing panels to determine its elastic characteristics. Results of these tests are shown as elastic-axis location and torsional stiffness in figure 19 and as structural influence coefficients in table III. The wing panel was supported between 40- and 70-percent root chord in the same manner in which it was mounted for the flight tests. The elastic-axis location varied from 38-percent chord at the root to the leading edge of the wing at about 70-percent span. Outboard of the 70-percent-span station the elastic axis is not shown, due to inaccuracy in determining the location introduced by large deflections and the small chord at wing tip stations.

Somewhat lower values of the lift-curve slope were shown by flight tests than by tests of reference 2. Wing deflection data determined from the static tests were used to compute the change in lift-curve slope due to aerodynamic loading on the wing panels. While some effect of aeroelastic deflection was noted, of the order of 1 percent, it was too small to account for a significant portion of the difference between the results of the two tests.

REFERENCES

1. Hall, Charles F.: Lift, Drag, and Pitching Moment of Low-Aspect-Ratio Wings at Subsonic and Supersonic Speeds. NACA RM A53A30, 1953.

2. Heitmeyer, John C., and Stephenson, Jack D.: Lift, Drag, and Pitching Moment of Low-Aspect-Ratio Wings at Subsonic and Supersonic Speeds - Plane Triangular Wing of Aspect Ratio 4 with NACA 0005-63 Section. NACA RM A50K24, 1951.

3. Fournier, Paul G.: Wind Tunnel Investigation of the Aerodynamic Characteristics in Pitch and Sideslip at High Subsonic Speeds of a Wing-Fuselage Combination Having a Triangular Wing of Aspect Ratio 4. NACA RM L53G14a, 1953.

4. Holdaway, George H.: Comparison of the Aerodynamic Characteristics at Transonic Speeds of a Plane Wing and a Cambered and Twisted Wing, Both Having 45° of Sweepback and Aspect Ratio of 6. NACA RM A53B16, 1953.

5. White, Maurice D.: Effect of Camber and Twist on the Stability Characteristics of Models Having a 45° Swept Wing as Determined by the Free-Fall Method at Transonic Speeds. NACA RM A52F16, 1952.

6. White, Maurice D.: A Flight Investigation at Transonic Speeds of the Aerodynamic Characteristics of a Model Having a Thin Unswept Wing of Aspect Ratio 3.1. NACA RM A54E12, 1954.

7. Holdaway, George H.: Comparison of Theoretical and Experimental Zero-Lift Drag-Rise Characteristics of Wing-Body-Tail Combination Near the Speed of Sound. NACA RM A53H17, 1953.

8. Tinling, Bruce E., and Lopez, Armando E.: The Effects of Horizontal-Tail Location and Size on Subsonic Longitudinal Aerodynamic Characteristics of an Airplane Model Having a Triangular Wing of Aspect Ratio 3. NACA RM A53L15, 1954.

9. Sleeman, William C., Jr., and Becht, Robert E.: Aerodynamic Characteristics of a Delta Wing With Leading Edge Swept Back 45°, Aspect Ratio 4, and NACA 65A006 Airfoil Section - Transonic Bump Method. NACA RM L9G22a, 1949.

10. Axelson, John A.: Downwash Behind a Triangular Wing of Aspect Ratio 3 - Transonic Bump Method. NACA RM A53I23, 1953.

11. Tobak, Murray, Reese, David E., Jr., and Beam, Benjamin H.: Experimental Damping in Pitch of 45° Triangular Wings. NACA RM A50J26, 1950.

12. Purser, Paul E.: Notes on Low-Lift Buffeting and Wing Dropping at Mach Numbers Near 1. NACA RM L51A30, 1951.

13. Gillis, Clarence L.: Buffeting Information Obtained from Rocket-Propelled Airplane Models Having Thin Unswept Wings. NACA RM L50H22a, 1950.

TABLE I.- DIMENSIONS OF MODEL

Gross weight, lb	1800 to 1845
Moment of inertia, about Y-axis, slug-ft^2	893 to 906
Center of gravity	0.326$\bar{c}$ to 0.388$\bar{c}$
Wing	
Area, sq ft	30.1
Area, exposed panels, sq ft	23.1
Aspect ratio	4
Taper ratio	0
Span, ft	10.97
Mean aerodynamic chord, ft	3.66
Airfoil section	NACA 0005
Horizontal tail (all-movable, hinge-line perpendicular to model longitudinal axis)	
Area, sq ft (including 2.0 sq ft in fuselage)	6.0
Aspect ratio	4.5
Taper ratio	.20
Span, ft	5.21
Mean aerodynamic chord (including fuselage area) ft	1.36
Leading edge of mean aerodynamic chord	Station 153.6
Root chord, ft	1.96
Tip chord, ft	0.40
Airfoil section, parallel to stream	NACA 65006
Gap between tail and fuselage at 0° incidence, in.	1/16
Vertical tail (all-movable, differentially geared, hinge-line perpendicular to longitudinal axis of model)	
Area, (including 1.4 sq ft in fuselage) sq ft	3.3
Aspect ratio	5.1
Taper ratio	0.22
Span, ft	4.1
Mean aerodynamic chord (including area included in fuselage) ft	0.93
Leading edge, of mean aerodynamic chord	Station 151.0
Root chord, ft	1.34
Tip chord, ft	0.29
Airfoil section, perpendicular to quarter-chord line	NACA 65009
Gap between tail and fuselage at 0° deflection, in.	1/16
Fuselage	
Fineness ratio	12.4
Ordinate at station x (x = 8.0 to x = 139.4) in.	$r = 8.5[1 - (x-102/102)^2]^{3/4}$

TABLE II.- ORDINATES OF WING AIRFOIL SECTION NACA 0005

Station, percent chord	Ordinate, percent chord
0	0
1.25	.792
2.50	1.092
5.00	1.483
7.50	1.750
10.00	1.950
15.00	2.225
20.00	2.392
25.00	2.475
30.00	2.500
40.00	2.417
50.00	2.208
60.00	1.900
70.00	1.525
80.00	1.092
90.00	.600
95.00	.333
100.00	(.050)
100.00	.000
L.E. radius:	0.278

TABLE III.- STRUCTURAL INFLUENCE COEFFICIENTS

Loading Station	Deflection Gage Station										
	1	11	12	18	19	21	20	16	15	7	6
1	0.004	0.003	0.001	0.001	0.002	0.003	0.002	0.002	0.001	0	-0.001
2	.006	.008	.008	.008	.009	.013	.010	.008	.005	.002	.001
3	.003	.005	.007	.009	.013	.016	.013	.011	.008	.005	.002
4	.002	.005	.007	.010	.013	.017	.015	.011	.009	.005	.002
5	.001	.004	.007	.010	.014	.016	.015	.012	.010	.008	.010
6	.001	.003	.004	.006	.010	.010	.010	.007	.007	.010	.043
7	.001	.006	.010	.015	.022	.028	.052	.022	.021	.045	.006
8	.003	.010	.016	.025	.044	.040	.035	.029	.023	.017	.075
9	.004	.010	.017	.025	.037	.036	.023	.015	.015	.010	.004
10	.007	.015	.021	.025	.042	.039	.042	.023	.015	.010	.003
11	.005	.011	.010	.011	.016	.017	.020	.010	.006	.003	.002
12	.043	.011	.044	.020	.028	.028	.029	.037	.011	.007	.002
13	.008	.022	.030	.045	.060	.075	.060	.048	.032	.020	.007
14	.010	.038	.044	.080	.116	.144	.122	.100	.078	.044	.016
15	.003	.016	.022	.043	.069	.098	.082	.072	.090	.030	.010
16	.005	.020	.030	.057	.105	.130	.150	.138	.080	.035	.012
17	.012	.042	.068	.082	.190	.264	.210	.170	.114	.060	.020
18	.016	.052	.082	.132	.184	.210	.156	.080	.082	.044	.032
19	.005	.018	.030	.045	.108	.145	.100	.062	.038	.018	.006
20	.006	.024	.044	.072	.180	.440	.340	.146	.078	.036	.010
21	0	.025	.035	.065	.230	1.250	.385	.155	.090	.040	.005

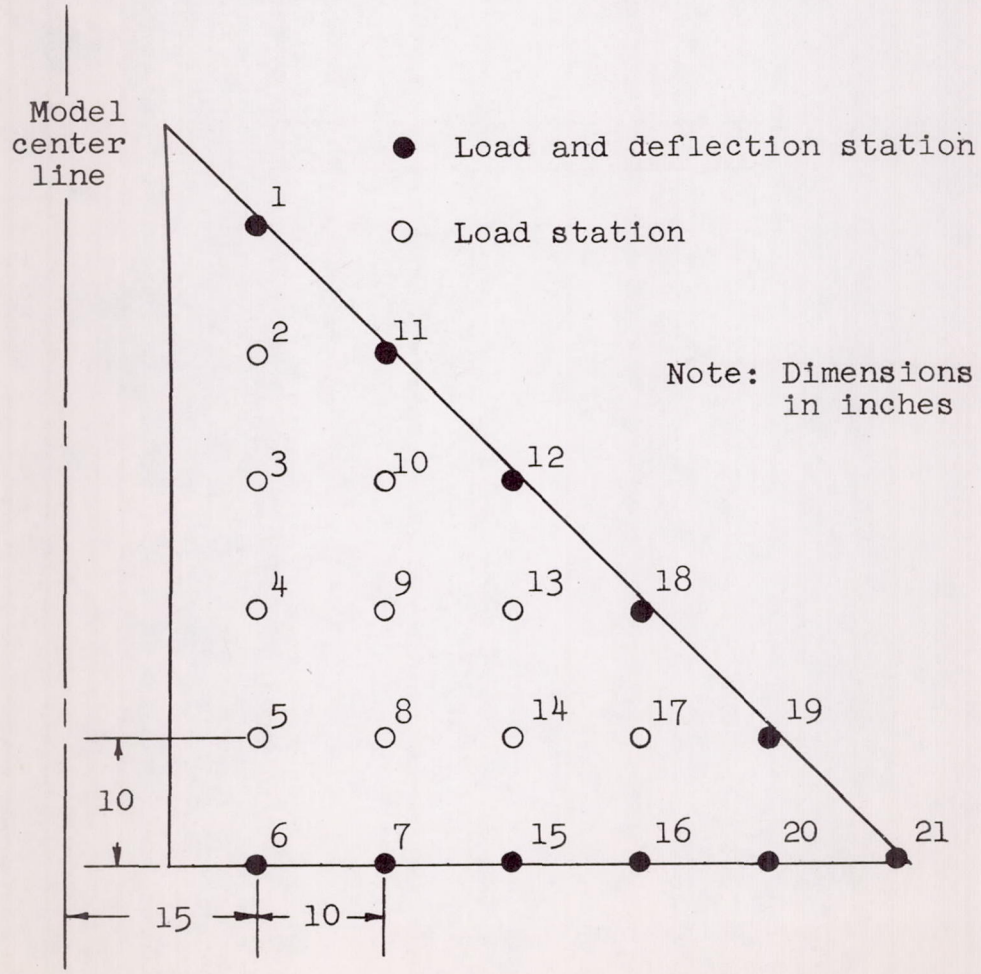

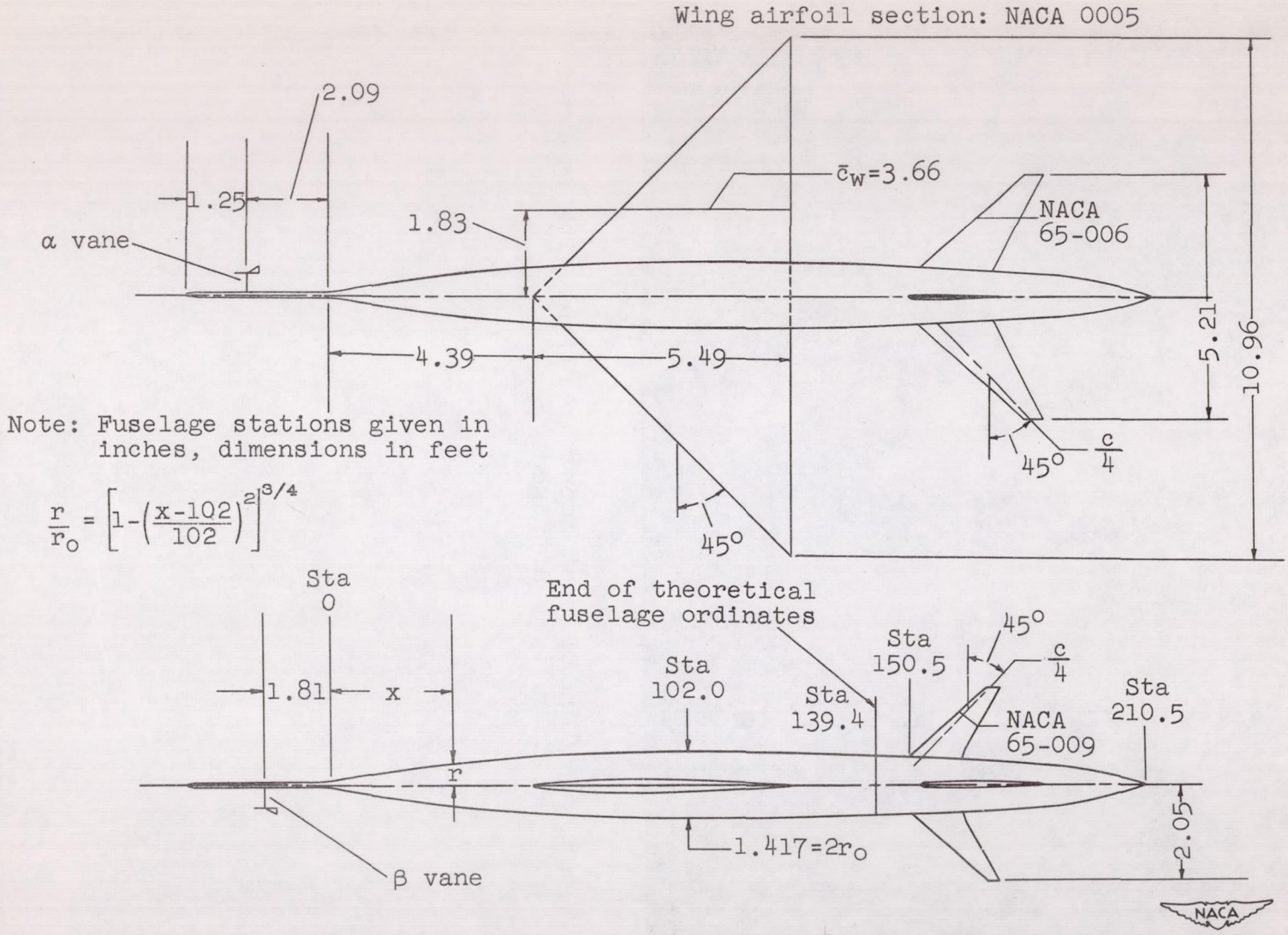

Figure 1.- Dimensional sketch of test model configuration.

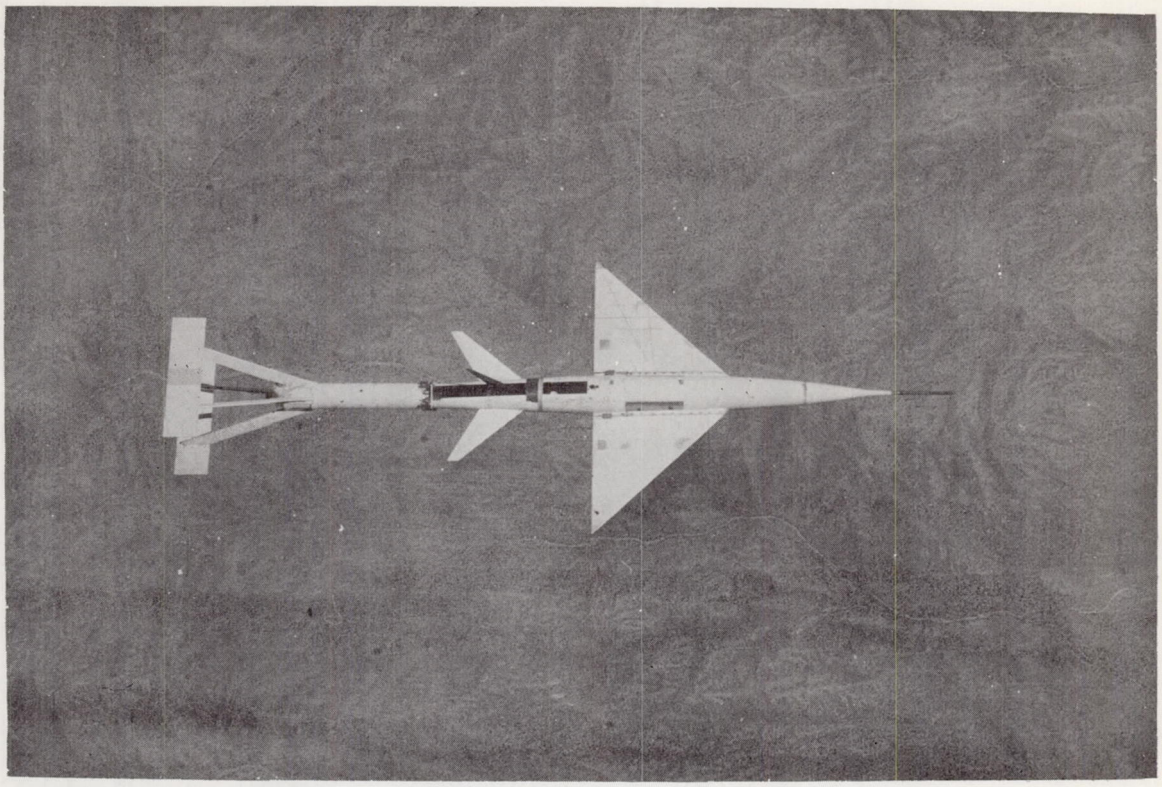

A-19784

Figure 2.- View of test model in flight with booster attached.

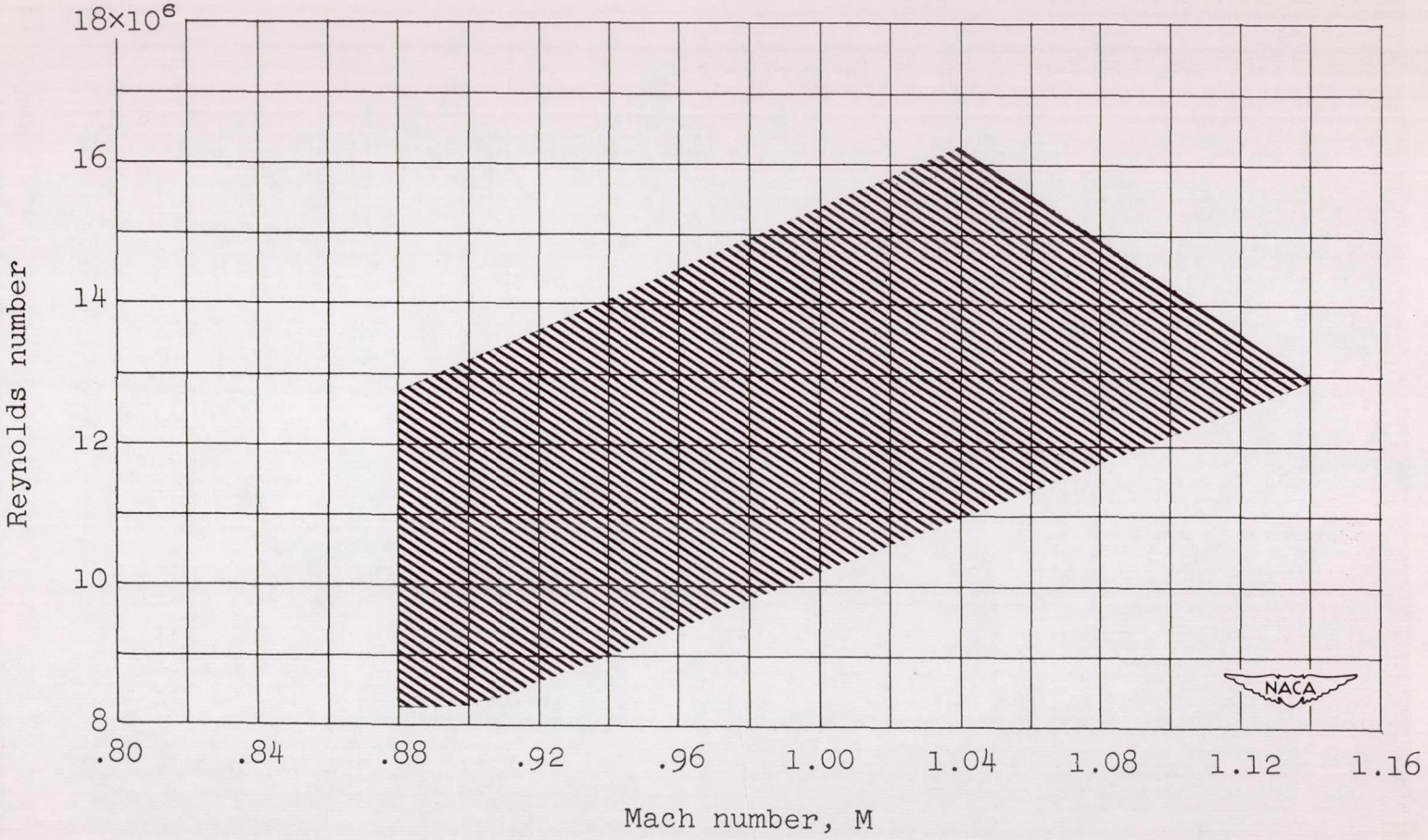

Figure 3.- Variation of Reynolds number with Mach number.

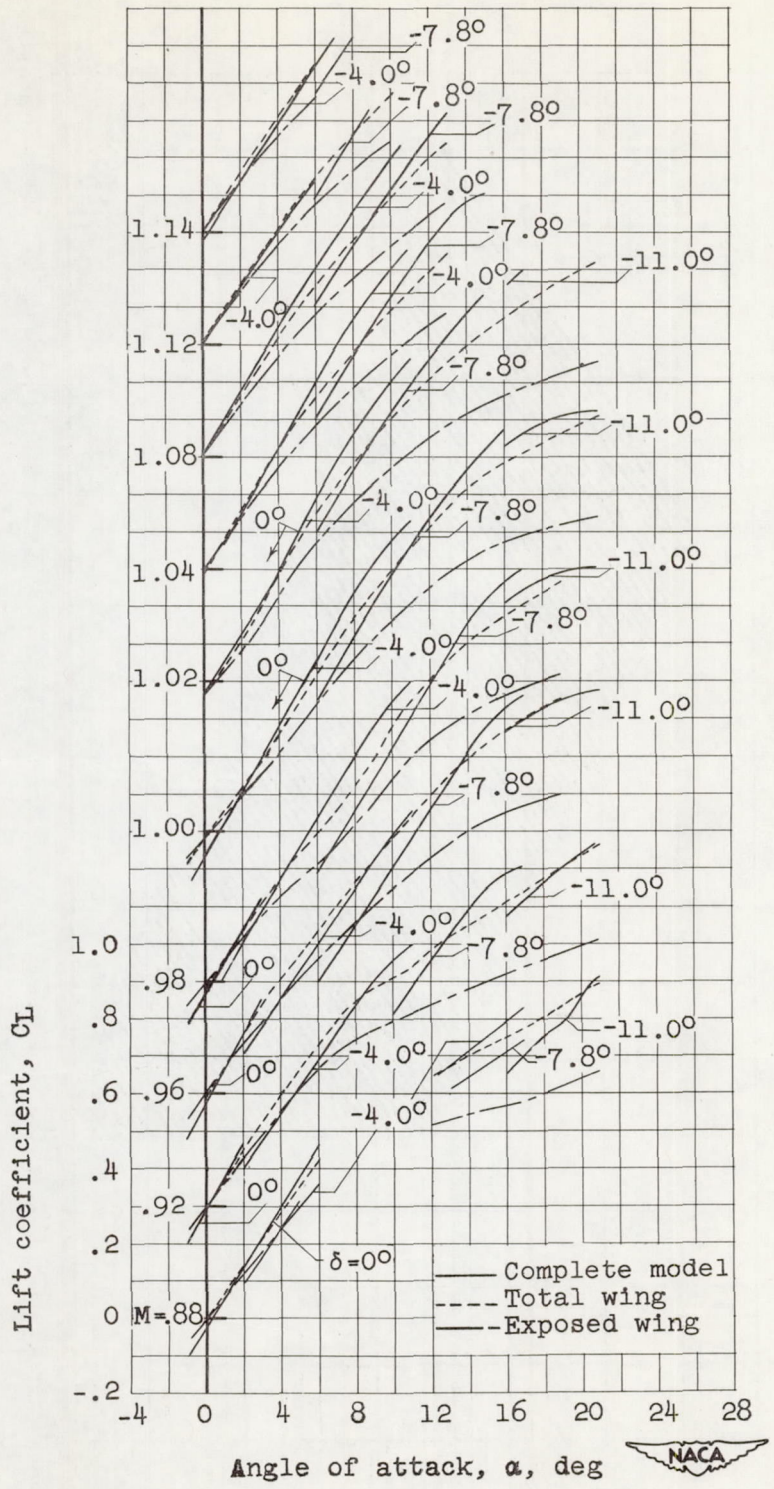

Figure 4.- Variation of lift coefficient with angle of attack for various model components.

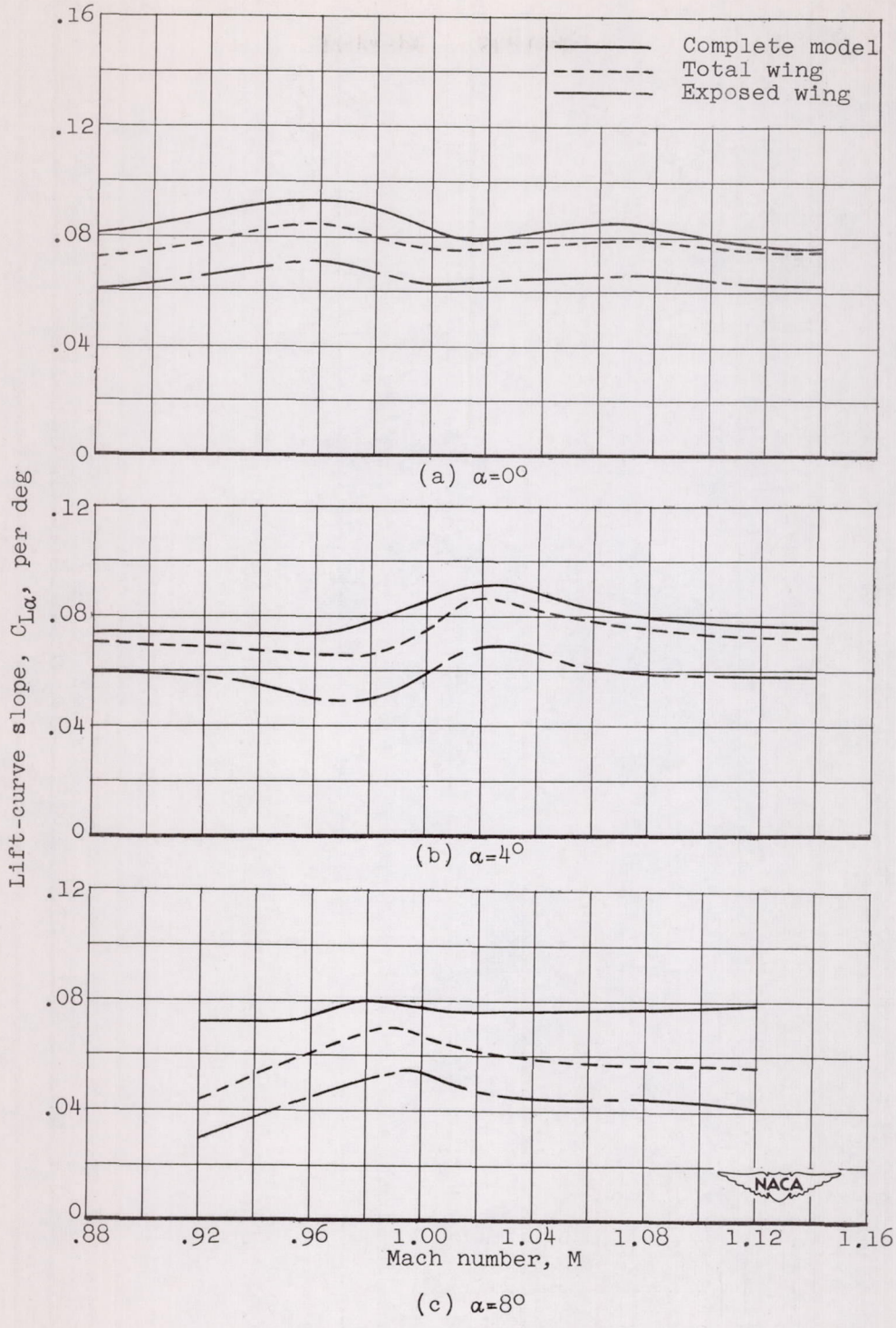

Figure 5.- Variation with Mach number of lift-curve slopes for various components of test model.

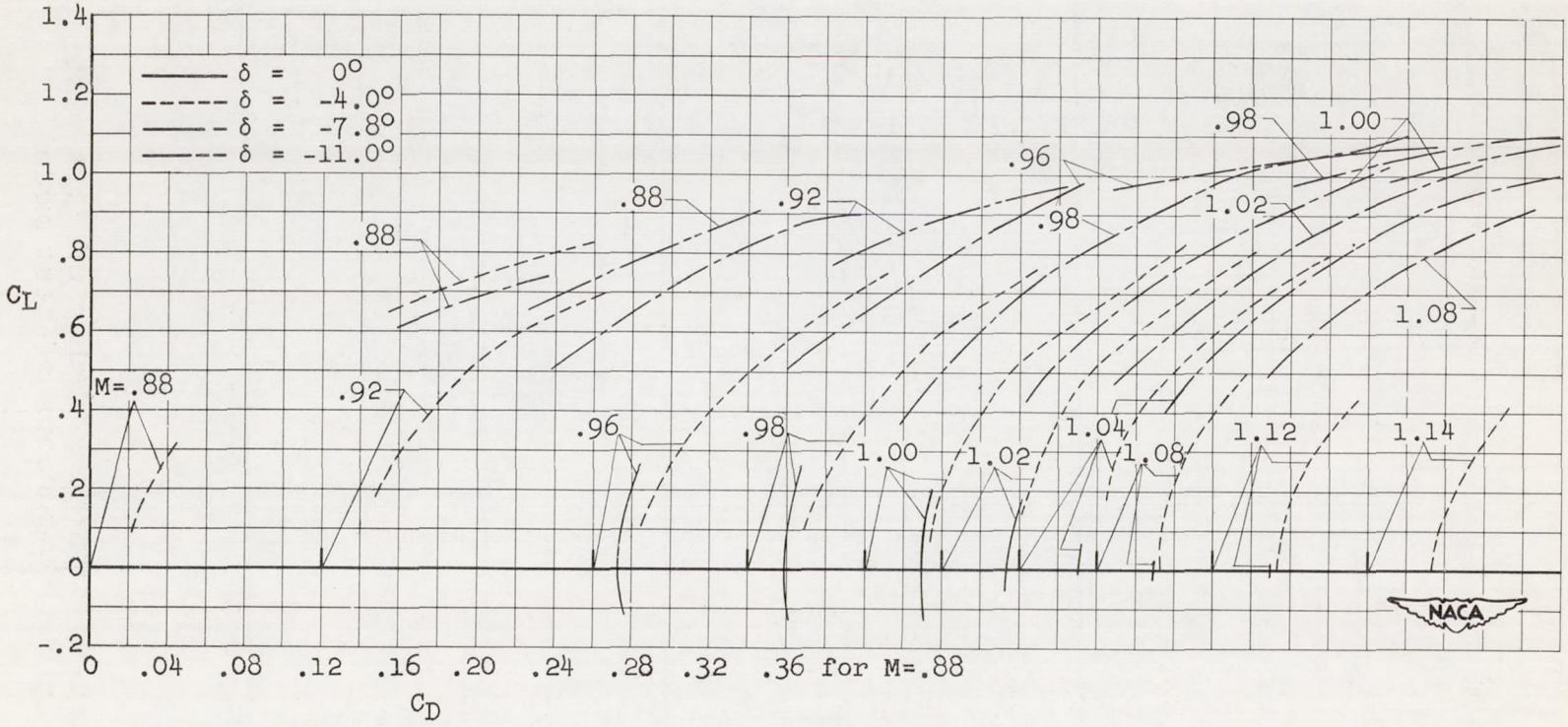

(a) Complete model.

Figure 6.- Variation of drag coefficient with lift coefficient for complete model and for the wing at various Mach numbers.

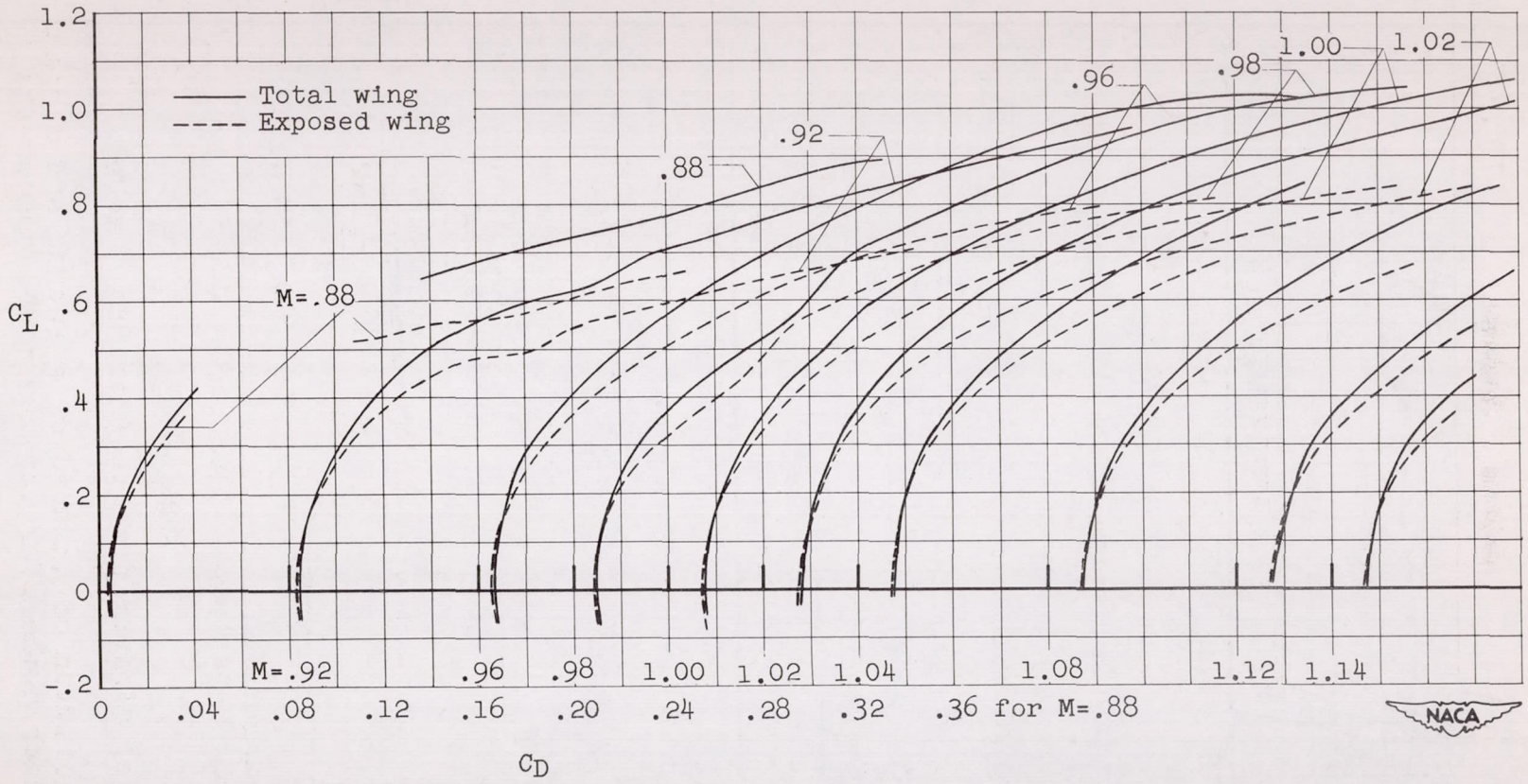

(b) Wing.

Figure 6.- Concluded.

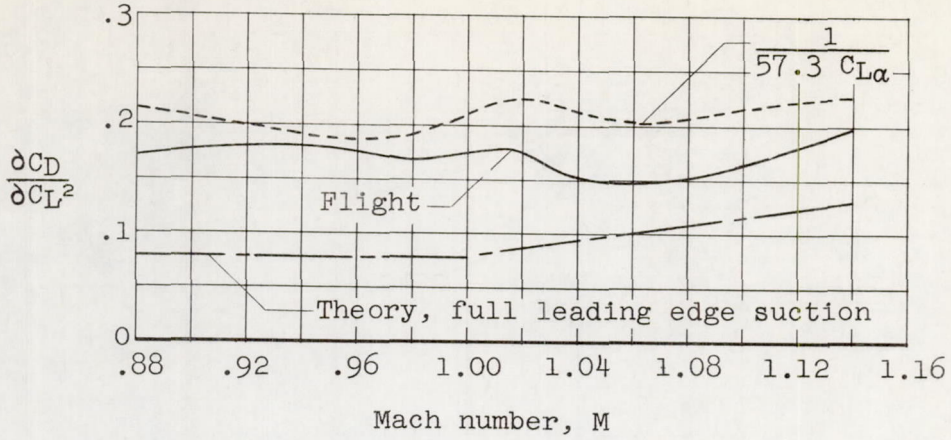

(a) Drag rise with lift - model.

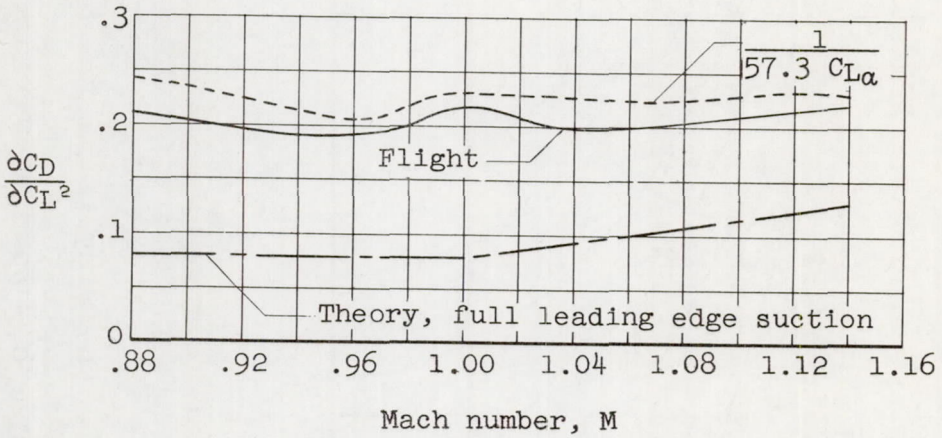

(b) Drag rise with lift - wing.

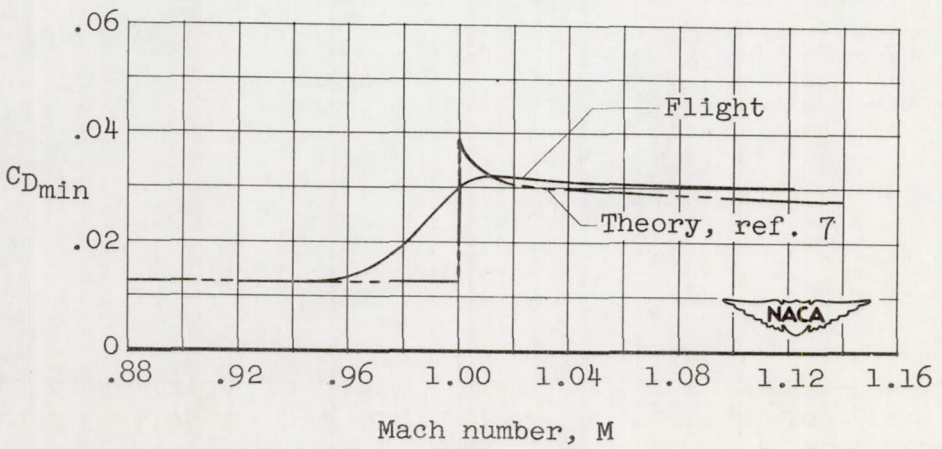

(c) Minimum drag coefficient - model.

Figure 7.- Variation of induced drag factor and minimum drag with Mach number for various model components.

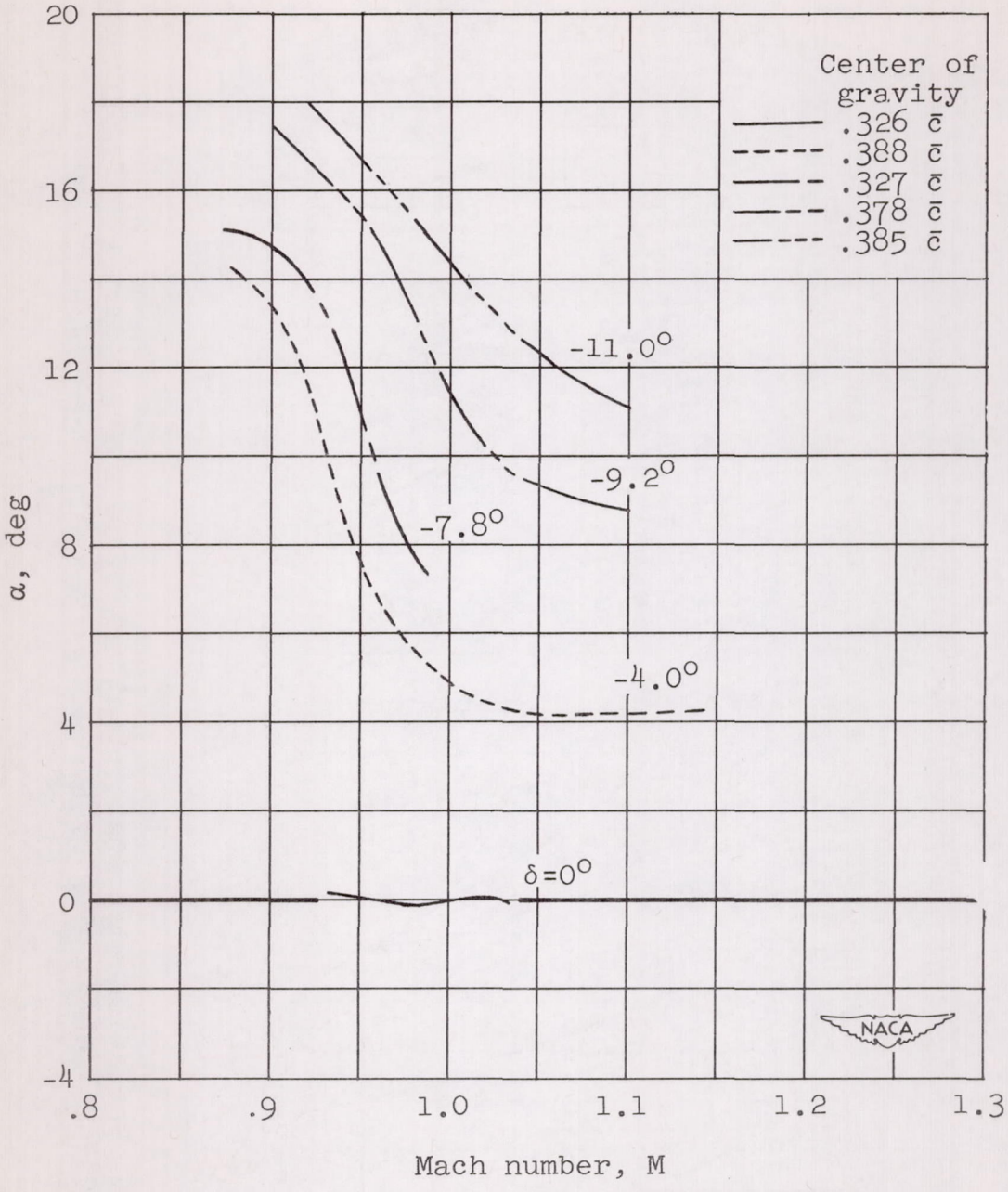

Figure 8.- Variation with Mach number of trim angle of attack for several tail settings and center of gravity positions.

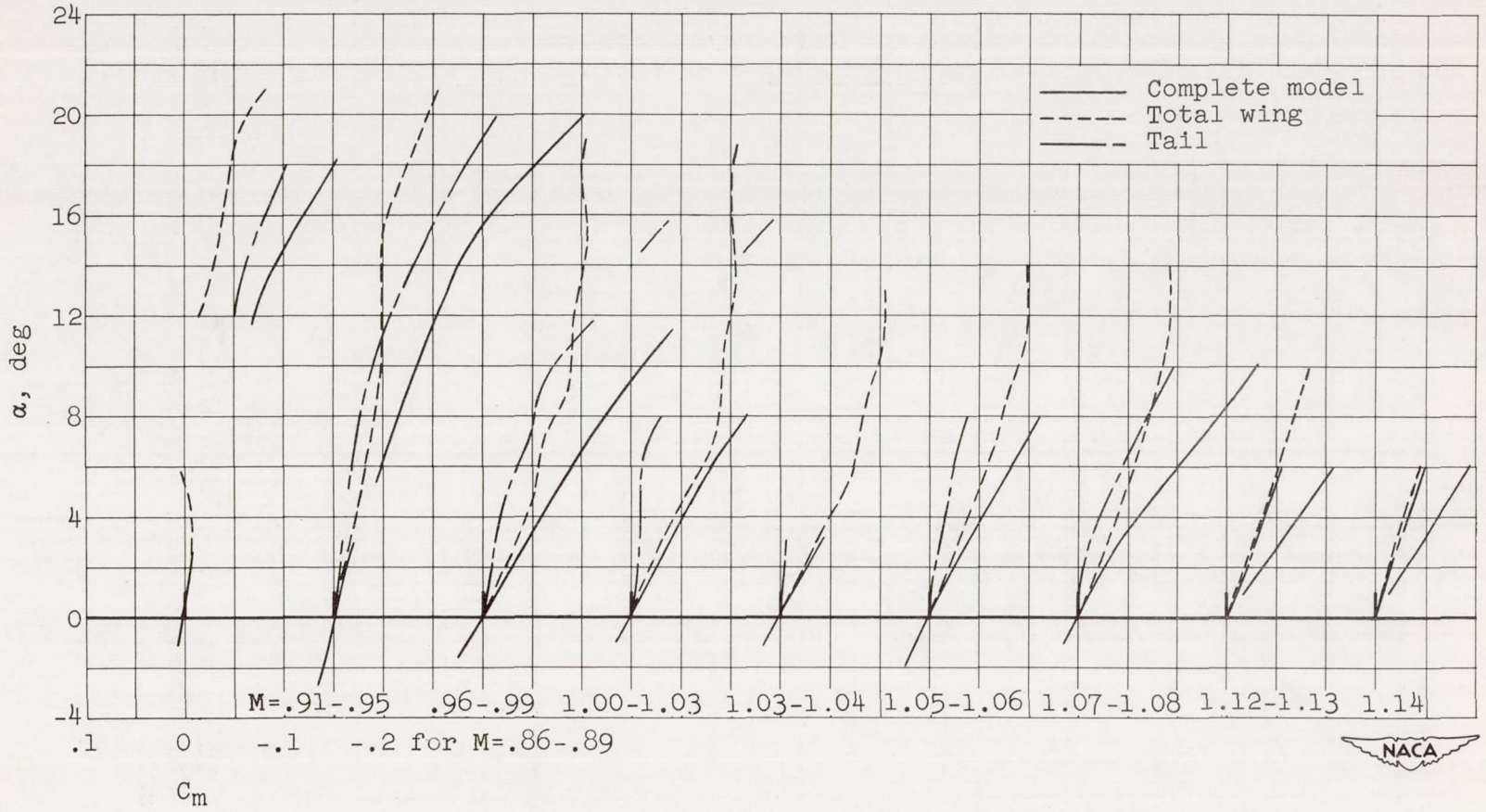

Figure 9.- Variation with angle of attack of pitching-moment coefficient of several model components; $\delta=0^{o}$, center of gravity at $0.388\bar{c}$.

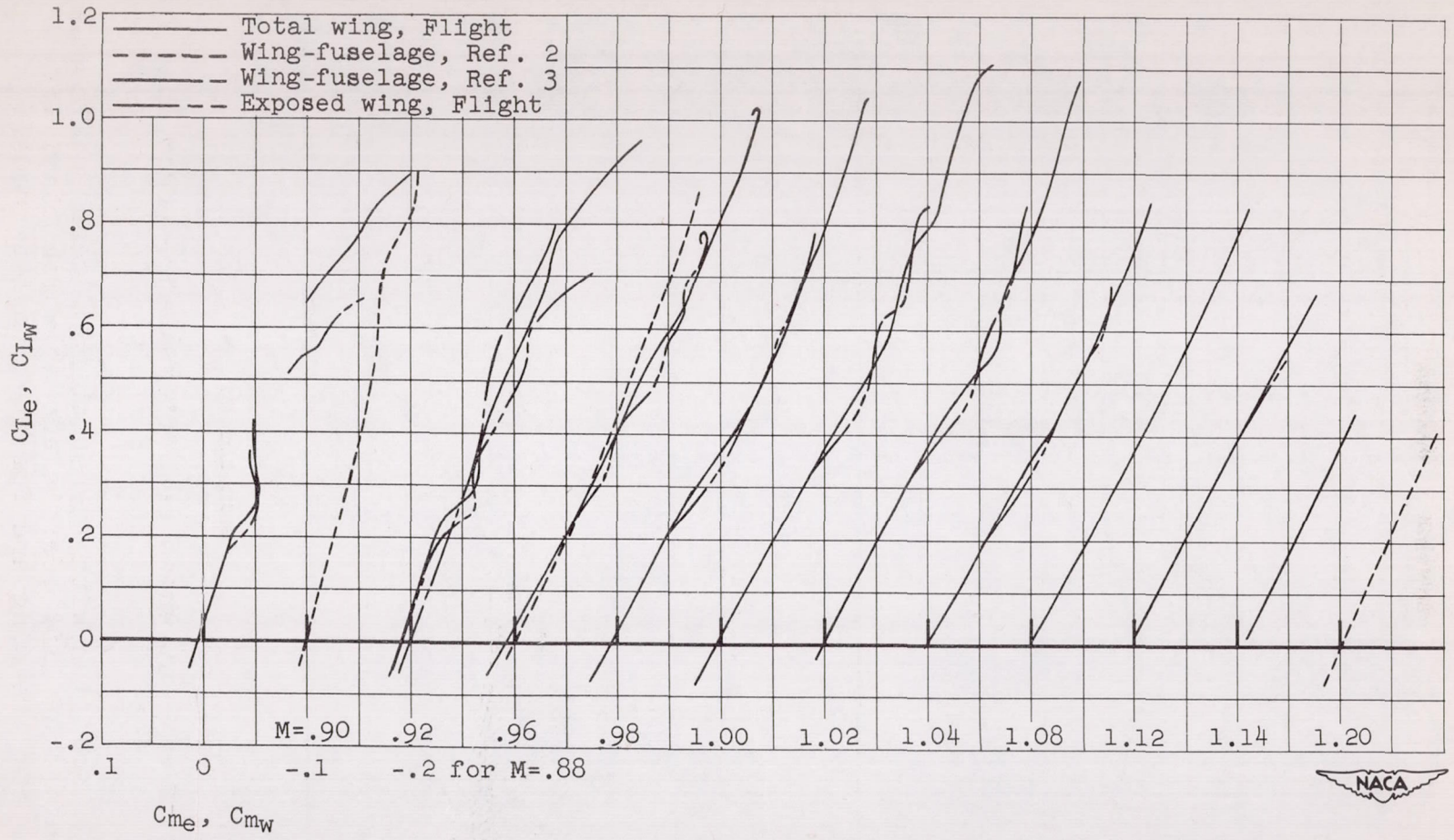

Figure 10.- Variation of pitching moment with lift coefficient for model wing; center of gravity at 0.25$\bar{c}$.

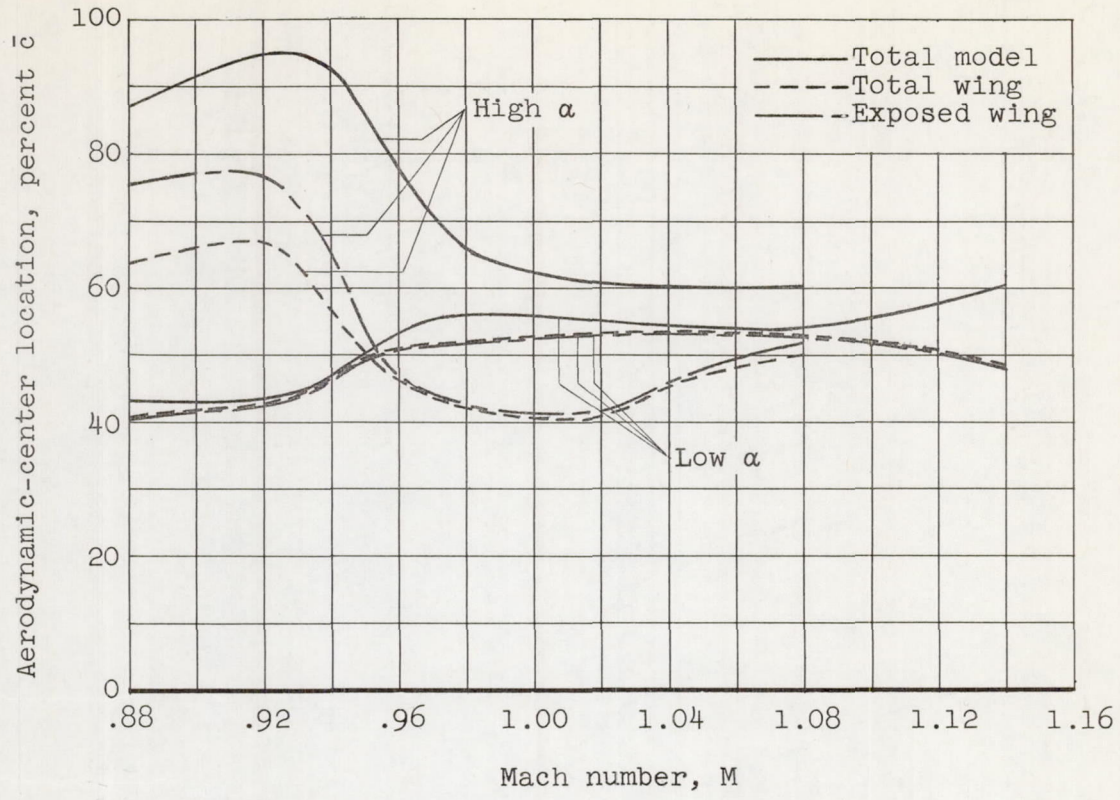

(a) Aerodynamic-center location.

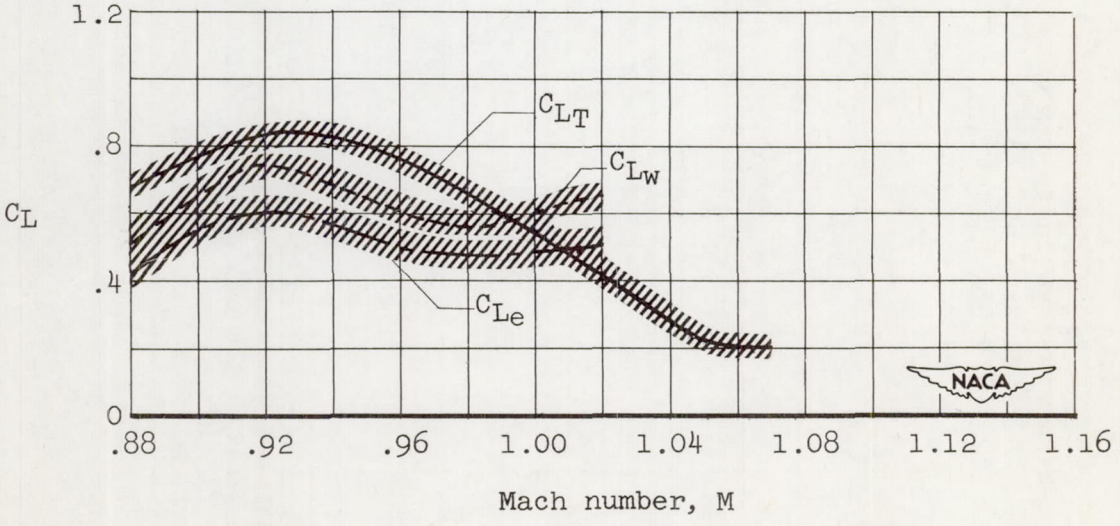

(b) Values of C_L at which stability changes from that for low C_L to that for high C_L.

Figure 11.- Variation with Mach number of aerodynamic-center location and of lift coefficient at which stability changes, for the wing and for the complete model.

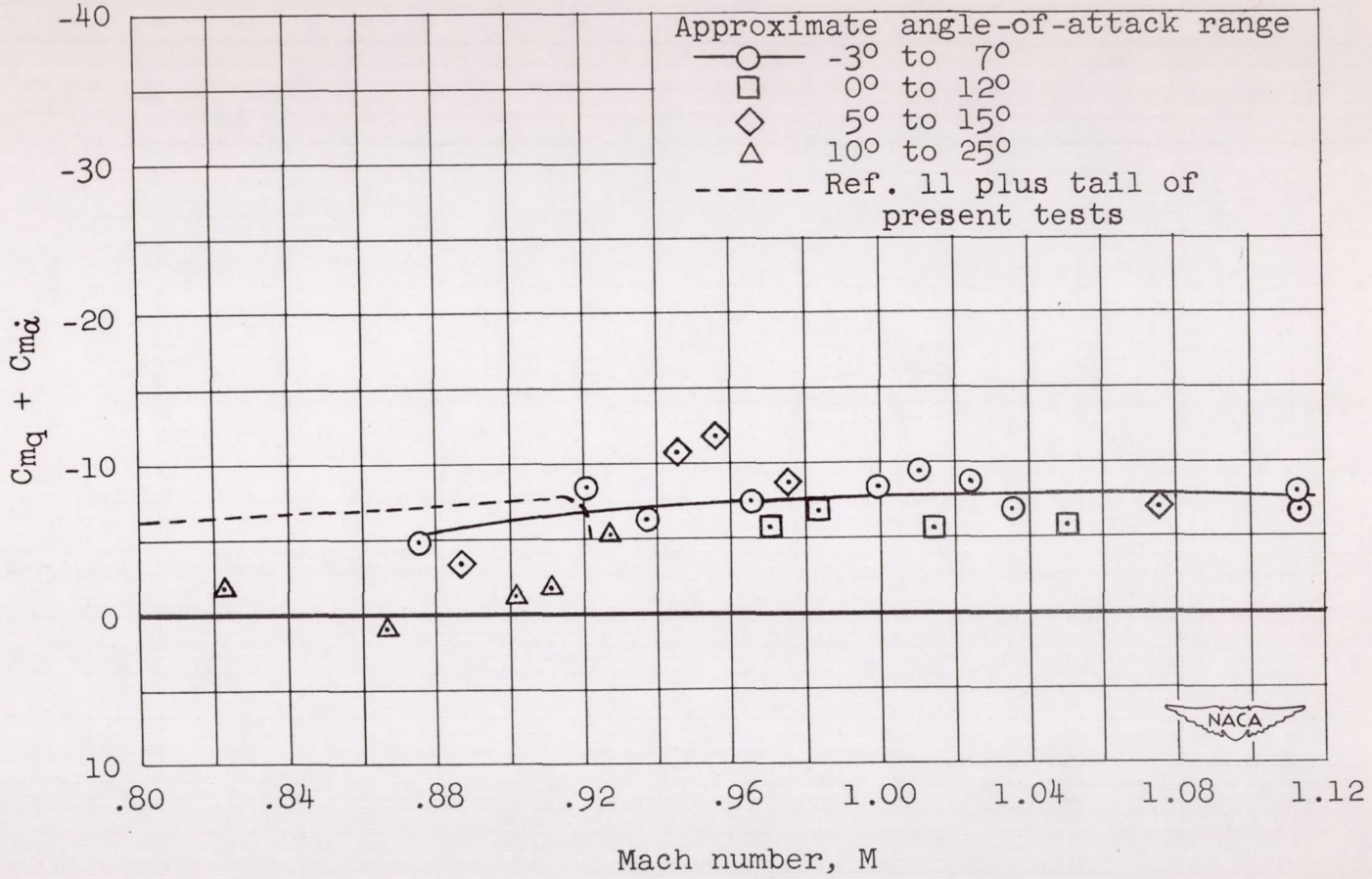

Figure 12.- Variation with Mach number of the damping-in-pitch parameter, $C_{m_q} + C_{m_{\dot{\alpha}}}$.

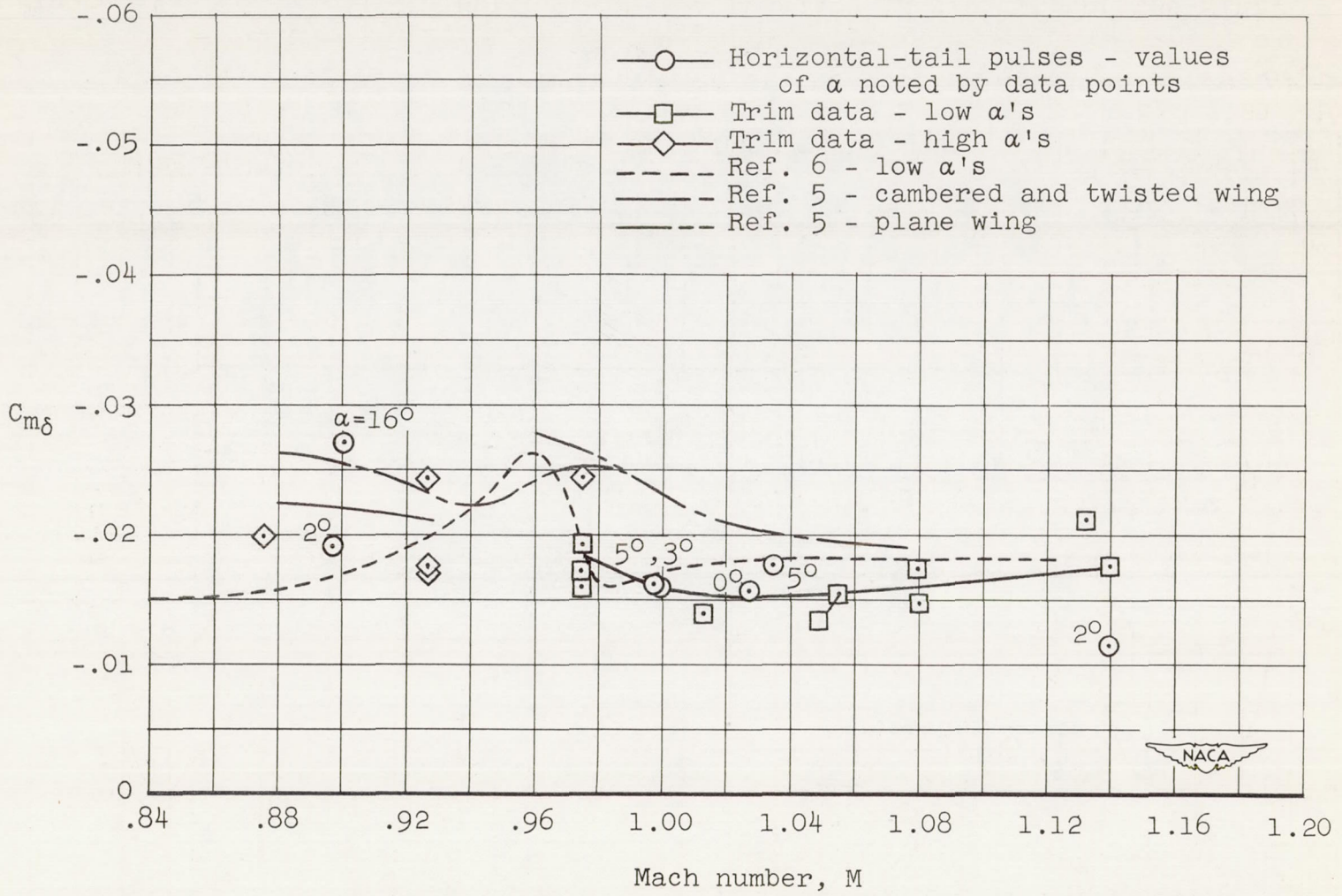

Figure 13.- Variation with Mach number of horizontal-tail-effectiveness parameter, C_{m_δ}; center of gravity, 0.388$\bar{c}$.

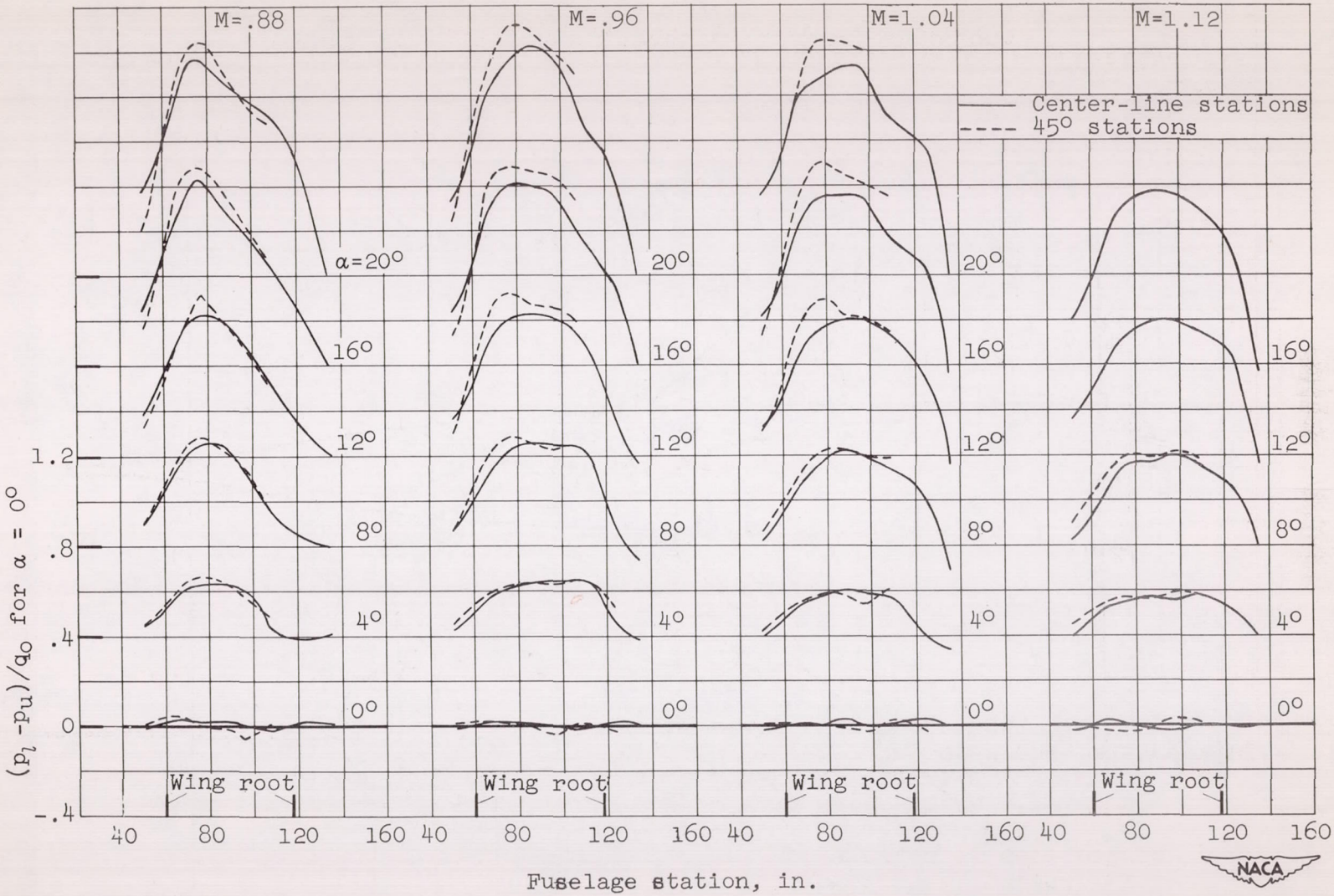

Figure 14.- Loading distribution over the fuselage in vicinity of the wing.

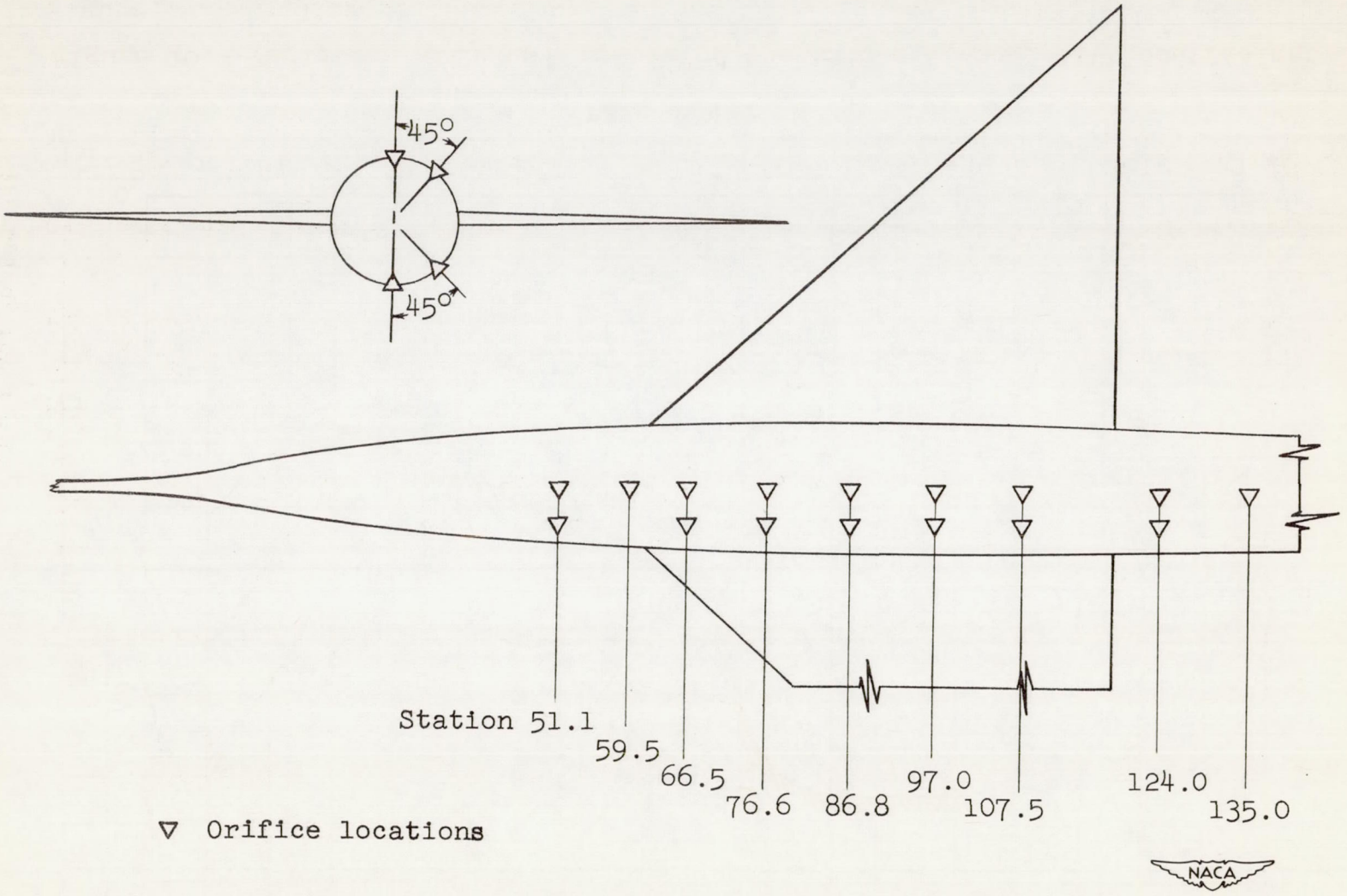

Figure 15.- Fuselage pressure orifice locations.

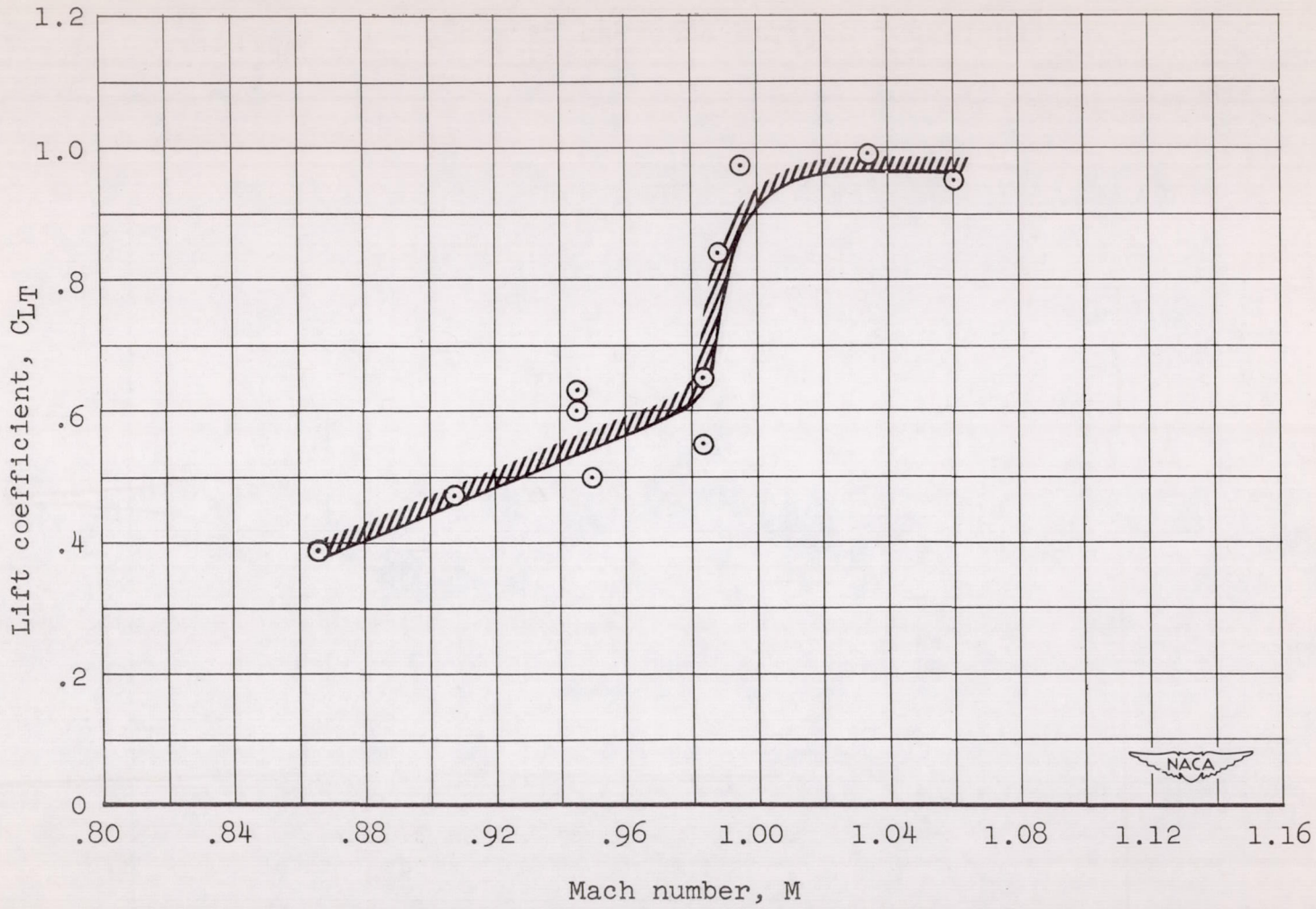

Figure 16.- Variation with Mach number of the complete model lift coefficient above which buffeting occurred.

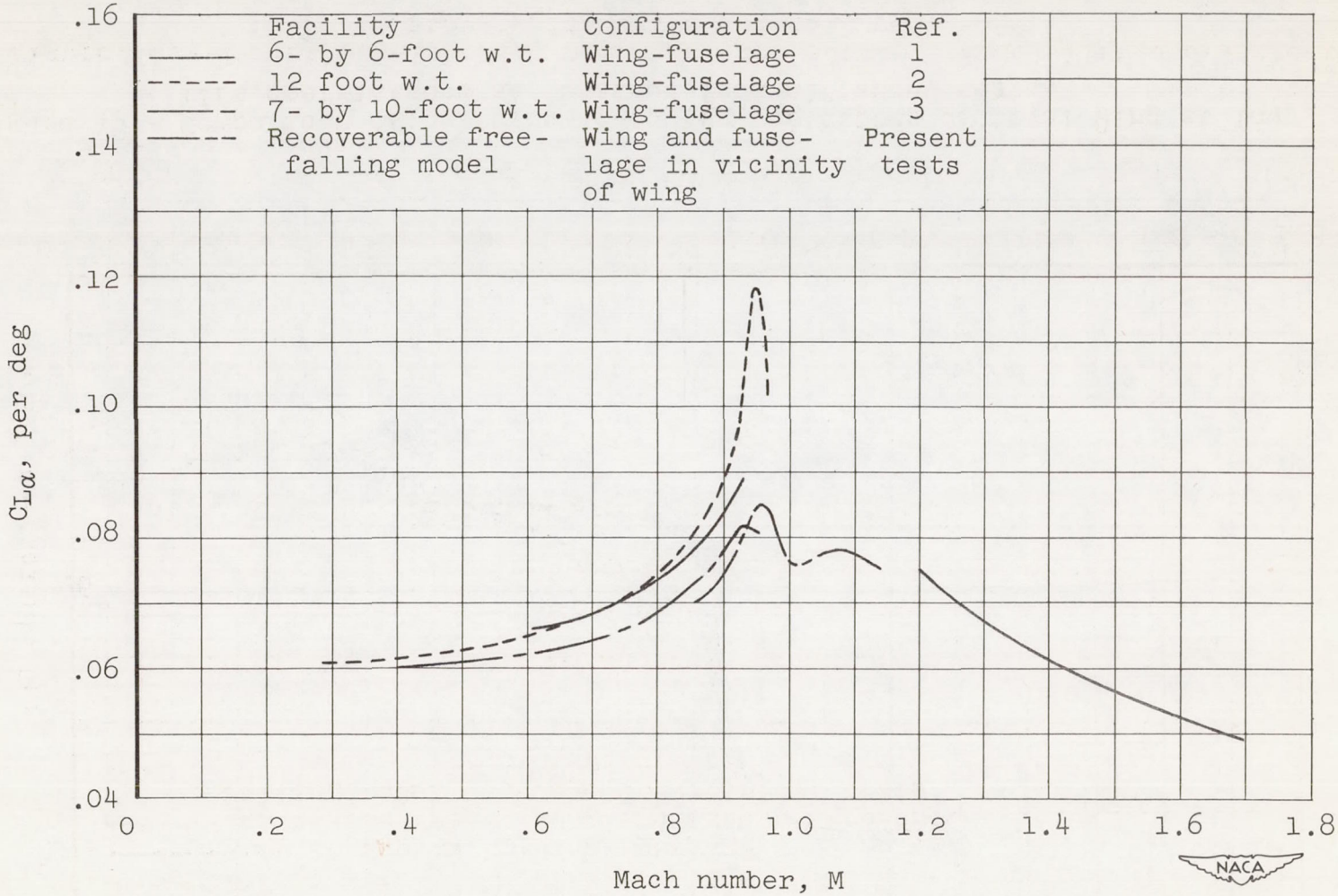

Figure 17.- Comparison of lift-curve slopes at zero lift for total wing as obtained from different tests.

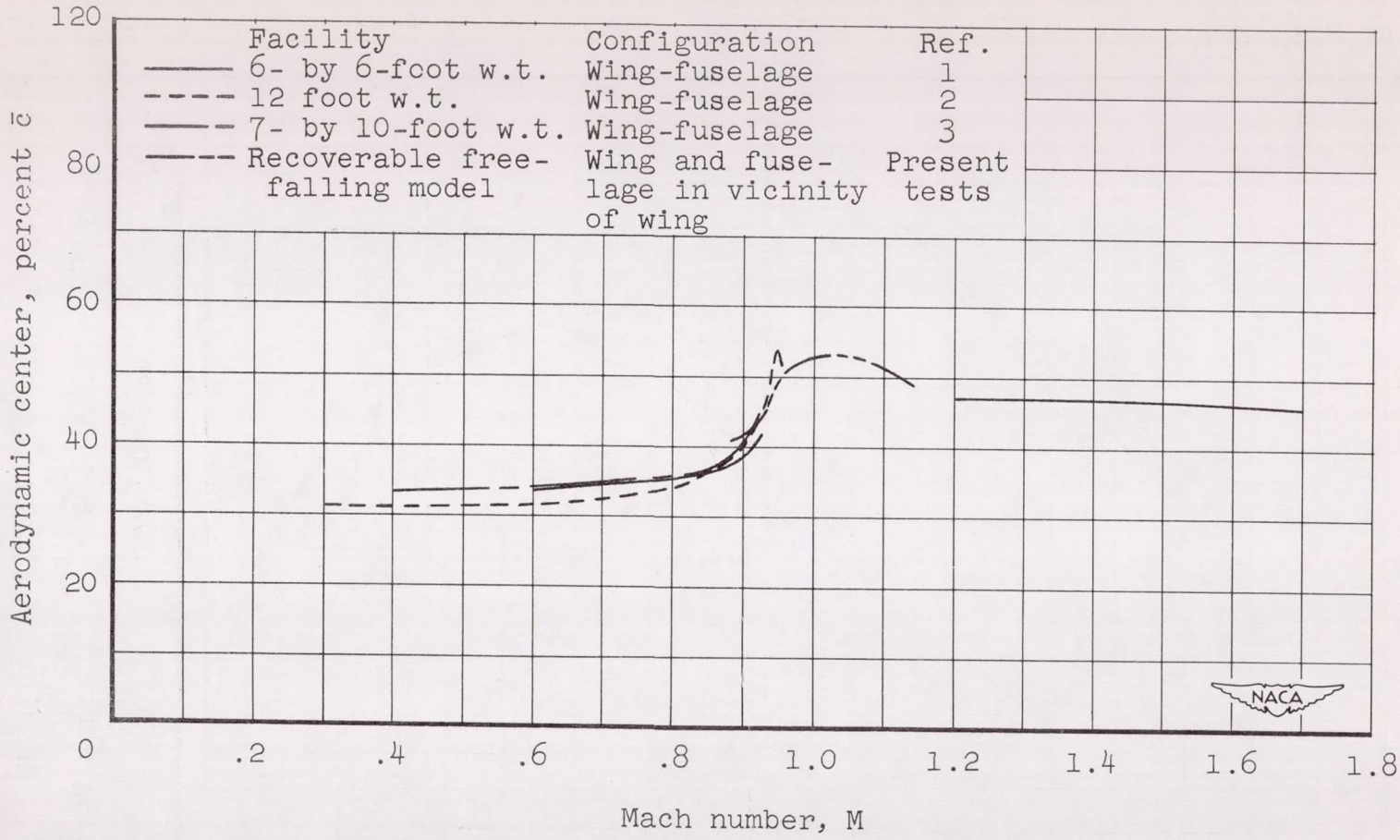

Figure 18.- Comparison of aerodynamic-center variations of total wing at low lift coefficients as obtained from different tests.

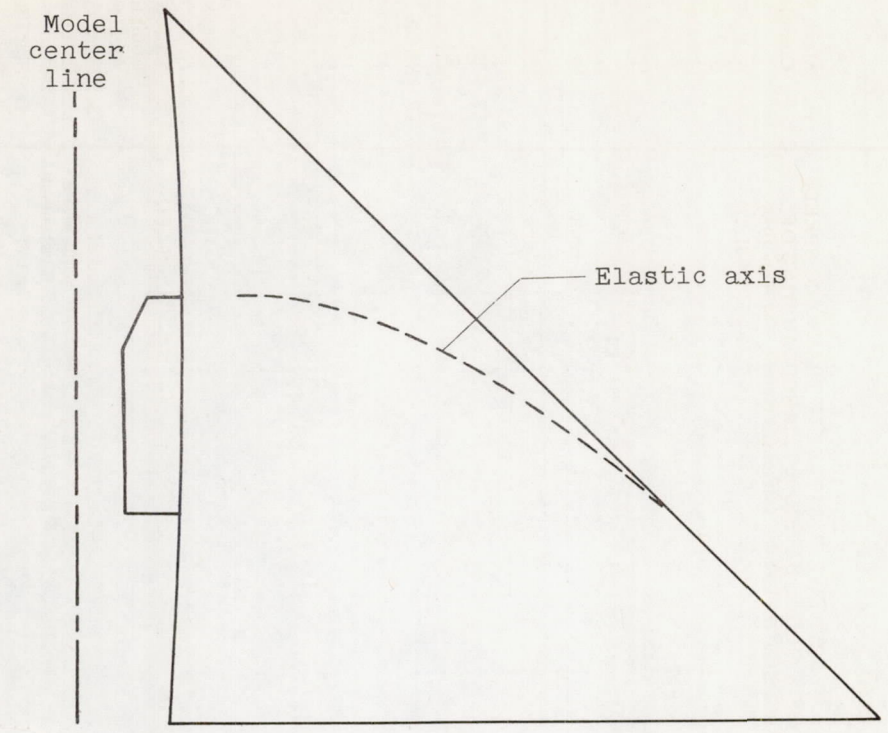

(a) Elastic-axis location.

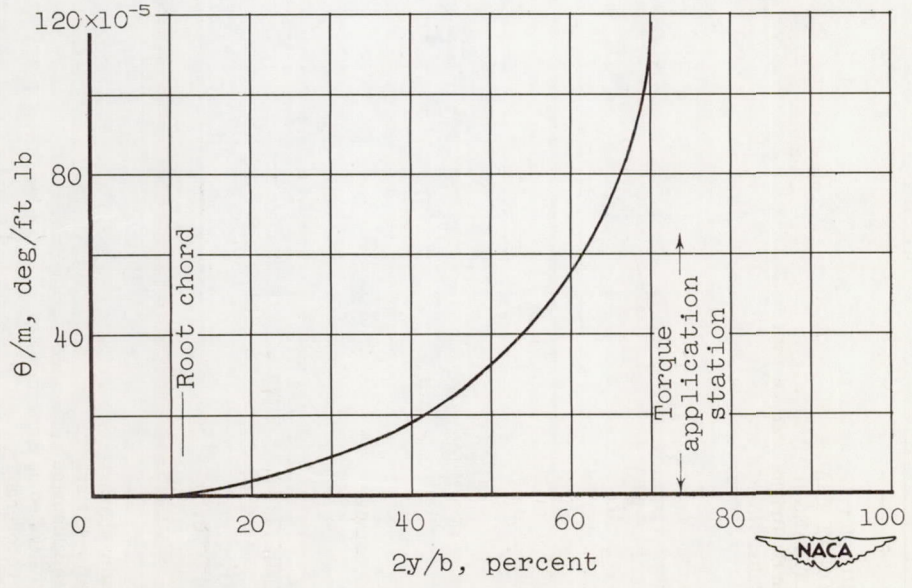

(b) Twisting deflections due to couple applied near tip.

Figure 19.- Results of ground tests to determine elastic characteristics of test wing.